AIAA JOURNAL
Vol. 38, No. 4, April 2000

Review of Planar Multiple-Component Velocimetry in High-Speed Flows

M. Samimy
Ohio State University, Columbus, Ohio 43210-1107
and
M. P. Wernet
NASA John H. Glenn Research Center at Lewis Field, Cleveland, Ohio 44135

High-speed flows encountered in most applications typically have very high Reynolds numbers and are often highly turbulent. Even in a laboratory-scale high subsonic or supersonic (high-speed) flow, velocities could vary over 3 orders of magnitude, and the turbulence spatial and temporal scales could span over 4–5 orders of magnitude. Exploring detailed physics of such flows presents major challenges to both experimental and computational researchers. An ultimate velocimetry technique would provide detailed, accurate, volumetric, real-time velocity data in such flows. With that being the goal, currently there are two planar velocimetry techniques that are developing rapidly into very useful tools with the potential of providing accurate velocity information in high-speed flows. The techniques are planar Doppler velocimetry (PDV) and particle imaging velocimetry (PIV). Whereas PDV has been under development for a relatively short period of time and is becoming a powerful technique, more accurate in high-speed flows, PIV is an established technique in low-speed flows and is now breaking ground in high-speed flows. The purpose of this review is to provide detailed background on these two techniques, to discuss the strengths and constraints of each technique, and to outline the areas in need of further improvement and development. The aims are to assist the novice users in their proper usage and to help those who are in the process of deciding which technique is more appropriate in their specific applications.

Nomenclatures

D	= jet diameter
f_{mon}	= laser frequency monitoring
I/I_0	= filter transmission coefficient
$\boldsymbol{o}$	= unit vector in the laser light propagation direction
P_{I2}	= iodine partial pressure in the filter cell
P_{N2}	= nitrogen partial pressure in the filter cell
$\boldsymbol{s}_1, \boldsymbol{s}_2, \boldsymbol{s}_3$	= unit vectors toward the detectors/observers 1, 2, and 3
T_{cell}	= filter cell temperature
T_{I2}	= filter side arm temperature
$\boldsymbol{V}$	= velocity vector
V_c	= jet centerline velocity
V_x, V_y, V_z	= velocities in the x, y, and z directions
α, β, γ	= angles that unit vectors $\boldsymbol{s}_1$, $\boldsymbol{s}_2$, and $\boldsymbol{s}_3$ make with the x coordinate (Fig. 9)
Δf_d	= Doppler shift
ν_0	= laser light frequency

Introduction

TO understand the dynamics of turbulent flows, one has to solve the Navier–Stokes (N–S) equations numerically or measure the flow properties experimentally. At the present time, even with the most powerful supercomputers and parallel processing machines, direct numerical simulation of the N–S equations is still limited to simple flows with very low Reynolds numbers. The ratio of the largest spatial or temporal scale to the smallest scale in a turbulent flow is proportional to Reynolds number to $\frac{3}{4}$ power ($\delta_{\max}/\delta_{\min} = \tau_{\max}/\tau_{\min} = Re^{3/4}$) (Ref. 1). If one takes a laboratory-scale unbounded flow such as a jet with a diameter of 25 mm (which is about 100 times smaller than the size of an actual jet engine nozzle), the

Mohammad (Mo) Samimy is a Professor and Associate Chair of Mechanical Engineering at the Ohio State University. He received his Ph.D. in 1984 in mechanical engineering from the University of Illinois at Urbana. His current research interests are gas dynamics, compressible turbulence, optical diagnostics, flow control, and aeroacoustics. Dr. Samimy has been a visiting research fellow at NASA John H. Glenn Research Center at Lewis Field, Wright Laboratories, NASA Ames/Stanford Center for Turbulence Research, and CEAT/LEA Laboratories at the University of Poitiers in France, and has lectured extensively in the United States and abroad. He was an Associate Editor of the *Journal of Propulsion and Power*, is currently an Associate Editor of the *AIAA Journal*, and the chair elect of the AIAA Aerodynamic Measurement Technology Technical Committee. Dr. Samimy is a fellow of the American Society of Mechanical Engineers, an Associate Fellow of AIAA, and author or coauthor of over 100 technical papers.

Mark Wernet received his Ph.D. in 1989 in chemical engineering from Case Western Reserve University in Cleveland, Ohio. He has been at NASA John H. Glenn Research Center at Lewis Field since 1985 in the Optical Instrumentation Technology Branch. His primary areas of interest are in the application of laser anemometry (both laser Doppler velocimetry and time of flight) and digital particle image velocimetry in turbomachinery and in microgravity. Dr. Wernet is currently a member of the AIAA Aerodynamic Measurement Technology Technical Committee.

Received 23 October 1998; revision received 27 August 1999; accepted for publication 3 September 1999.

Reynolds number is approximately 10^6, and the large-scale turbulence structures downstream of the jet core would be around 25 mm in size. The spatial resolution of the measurements must be better than $\delta_{\max}/Re^{3/4} = 0.0008$ mm $= 0.8\ \mu$m to resolve all of the scales. The minimum number of grid points required for a direct numerical simulation of such a flow is $Re^{9/4} \sim 3 \times 10^{13}$, and the minimum total number of points to resolve the timescale is $Re^3 = 10^{18}$. It is obvious that both the experimental and computational researchers have major challenges ahead of them. The only silver lining for experimentalists is that a tremendous amount of information could be obtained in a high-speed flow without resolving all of the scales. Obviously, the information in the measured data would be limited to the resolved scales. On the other hand, one has to resolve all of the scales in a direct numerical simulation to get accurate information. This is the major difference between experimental and direct numerical simulation work.

The focus of this review paper will be on optical techniques for velocity measurements. There are two conceptual optical methods that one can use to measure flow velocity. The first concept requires measuring the shift in the frequency of the illuminating laser light that is either scattered by the molecules in the flow[2] or the artificially seeded particles in the flow.[3] Some researchers have also used the Doppler shift of laser-induced fluorescing molecules for velocity measurement.[4] The idea of measuring the Doppler shift due to the motion of particles in the flow was originated by Cummins et al.[5] and Yeh and Cummins,[6] after the advent of narrow linewidth lasers. The widely used laser Doppler velocimetry (LDV), which is a point measurement technique, is based on this concept.[3] A new class of velocimetry technique based on a molecular filter, which was originated by Komine et al.[7] and Meyers and Komine,[8] has been developed within the past several years that can measure the Doppler shift of scattering particles on an illuminated plane.[7–33] This technique is called the planar Doppler velocimetry (PDV),[9–23] or Doppler global velocimetry (DGV).[7,8,24–33]

The second concept is based on measuring the transit time between two points of either tagged molecules in the flow[34–36] or artificially seeded particles in the flow.[37] The widely used particle imaging velocimetry (PIV) and its many variations are based on this concept.[37,38] A third planar technique, called scalar imaging velocimetry, which has been developed recently, first measures the conserved scalar field, then backs out the velocity component field along the local scalar gradient vector.[39,40] This technique is currently limited to flows with large Schmidt number and low Reynolds number.

As was discussed, high-speed flows, where the flows most often possess high Reynolds numbers, contain a very wide range of turbulence velocity, timescales, and length scales. Therefore, they require techniques with a large dynamic range both in velocity and space. For seeded-particle-based techniques, this means that one has to utilize very small and densely seeded particles. LDV, which has a large dynamic range in velocity and good pointwise spatial resolution, has been used successfully in such flows and has provided a wealth of turbulence data.[41–46] Unfortunately, LDV is a point measurement technique, which means that it requires an enormous amount of time to map out a flowfield and that it provides only mean velocity and turbulence statistical information.

In recent years, some work has also been carried out on line-writing using oxygen molecules.[35] These techniques are based on the transit time of tagged molecules and have two main advantages over LDV: 1) They are line measurement, rather than point measurement techniques. 2) They are based on molecules, rather than particles, thus they are free of problems such as particle fidelity and frequency response.

Over the past several years, more applications of planar two-component measurements in the illuminated plane PIV[47–50] and stereoscopic, three-component PIV[51] techniques have been used in high-speed flows. For correlation-based processing, high concentrations of small seed particles are required. Best results are obtained when the individual particle images are resolved, which can depend on the optical recording system resolution as much as on the physical size of the seed particles used. Submicron-sized seed particles are regularly employed in high-speed flows. The inherent spatial averaging resulting from correlation processing of small subregions across the recorded particle image frames limits the spatial dynamic range of the PIV technique. However, through proper optimization of the optical recording system, seed particle size and concentration, and data processing, PIV can yield accurate and reasonable spatial resolution measurements of high-speed flows.

In this review paper, details of PDV technique will be discussed first. It will be followed by the presentation of the PIV technique. Because PIV is an established technique that has been reviewed extensively in the literature, the focus will be on most recent advances pertinent to multiple-component and high-speed applications. Throughout the paper, PDV and PIV will be compared and contrasted to provide the reader an in-depth understanding of their capabilities, constraints, and advantages and disadvantages in various applications.

PDV

First, a comment on the name planar Doppler velocimetry is in order. The technique to be detailed herein is a planar technique that measures the Doppler shift in the scattered laser light, by particles in the flow, and thus the flow velocity. Therefore, the name PDV seems to be appropriate. Initially, however, Komine et al.[7] and Meyers and Komine[8] called it DGV. In earlier work from the laboratory of the first author of this review,[9–11] the technique was called filtered planar velocimetry. Smith et al.[15] called it absorption filter planar Doppler velocimetry. McKenzie[13,14] was first to call it PDV. Currently, both PDV[13–23] and DGV[24–33] are used for the technique. Thus, variations of fundamentally the same technique are used by different research groups, and it is called either PDV or DGV. This, to some degree, is similar to calling LDV laser Doppler anemometry (LDA) or laser velocimetry (LV) by different research groups.

Doppler Shift

The accurate measurement of the Doppler shift is at the heart of the PDV technique. Yeh and Cummins[6] and Cummins et al.[5] originated the idea of using the Doppler shift in the frequency of the light scattered by particles or molecules in the flow to measure the flow velocity. The Doppler shift equation is given by

$$\Delta f_d = [(\boldsymbol{s} - \boldsymbol{o})/\lambda] \cdot \boldsymbol{V} \tag{1}$$

where $\boldsymbol{s}$ is the unit vector toward the observer/detector, $\boldsymbol{o}$ is the unit vector in the propagation direction of the laser light, $\boldsymbol{V}$ is the velocity vector of the light-scattering fluid element/particle, and λ is the wavelength of the laser light (refer to Fig. 1). The measured velocity component is in the shown $(\boldsymbol{s}-\boldsymbol{o})$ direction, which can be oriented to a direction that an application might prefer.[16,20] Obviously, the maximum Doppler shift will be realized if $\boldsymbol{s}$, $\boldsymbol{o}$, and $\boldsymbol{V}$ are all aligned, and $\boldsymbol{s}$ and $\boldsymbol{o}$ are in the opposite directions. This maximum Doppler shift is $2|\boldsymbol{V}|/\lambda$. For a visible range laser operating at a wavelength of 532 nm, which is the second harmonic of Nd:YAG laser that is typically used with PDV, and for a supersonic flow velocity of 500 m/s, the maximum Doppler shift is only about 1.9 GHz. This Doppler shift is negligible in comparison with the visible laser light frequency of approximately 5.6×10^5 GHz. Therefore, the direct measurement of the frequency change in the laser light due to the Doppler shift presents a challenge. In the development stages of the

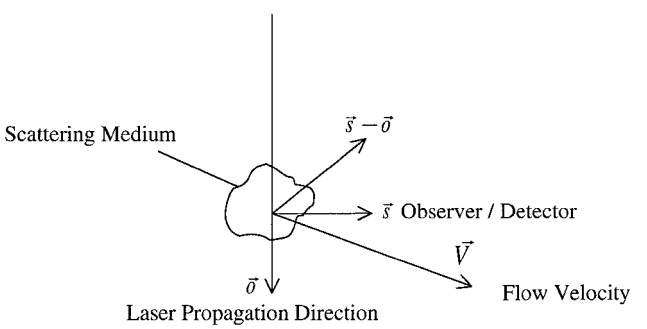

Fig. 1 Schematic of laser light-scattering by particles and the associated vectors for the Doppler shift calculation.

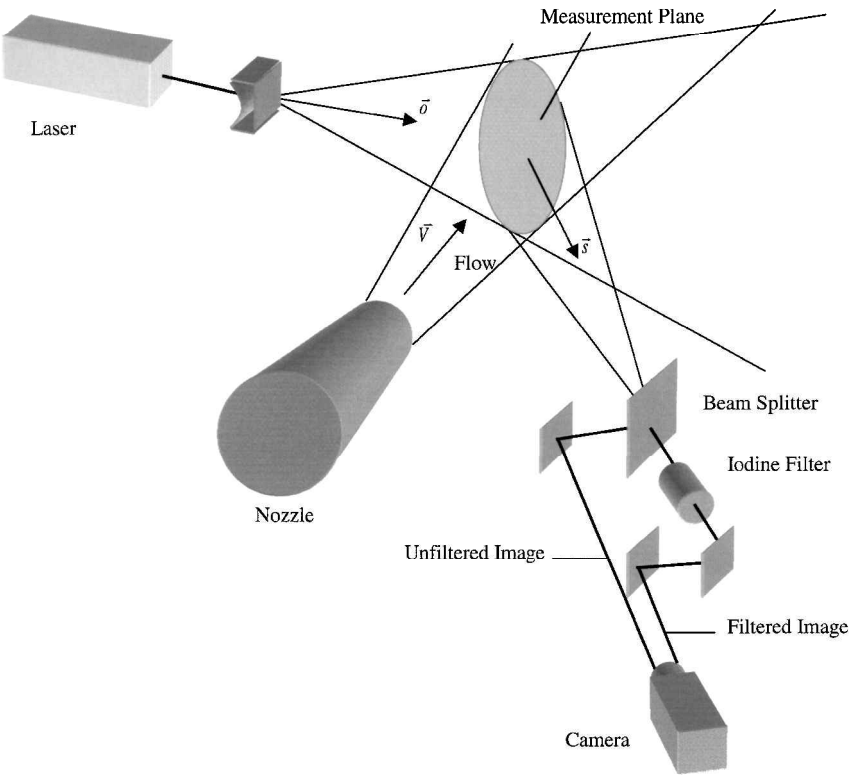

Fig. 2 Schematic of a one-camera-based single-component PDV system.

LDV technique, various configurations were used to utilize the optical beating or heterodyning of the scattered light with the original reference light to extract the Doppler shift.[3] The current configuration for LDV is the dual-beam configuration, which forms a set of either stationary or moving fringes in the measurement volume. In this configuration, however, the velocity of the scattering particles can be obtained without resorting to the Doppler shift, by knowing the distance between two fringes and the measurement of the time that takes for a particle to travel this distance. This is the reason for some researchers to drop the term Doppler from LDV or LDA and to call it simply LV or laser anemometry.

Unfortunately, extending the techniques that have been used so successfully to measure the Doppler shift in LDV to extract the velocity of the light-scattering particles in the flow and, thus, the velocity of the flow from its point measurement status to planar measurement is not feasible. Therefore, DGV or PDV, which is a new class of velocity measurement technique that measures the Doppler shift using a molecular filter, was originally proposed by Komine et al.[7] and Meyer and Komine[8] and has been developed over the past several years. First, an overview of the PDV technique will be provided, then its main components will be discussed.

Overview of PDV

Figure 2 represents a typical simple PDV system in which the laser light shown in Fig. 1 is formed into a sheet and a nonpolarizing beam splitter is used to split the scattered light into two beams. Then both beams are focused onto a single camera, after passing one of the beams through a molecular filter. The idea of putting both the filtered and unfiltered signal in a single detector, thus reducing the number of detectors by half, is a recent welcome development in the PDV technique.[13–19] In this setup, when the intensity of the filtered light is normalized with the intensity of the unfiltered light, the Doppler shift in the scatter light, or the component of flow velocity at $(\boldsymbol{s}-\boldsymbol{o})$ direction with a magnitude of $|(\boldsymbol{s}-\boldsymbol{o})\cdot\boldsymbol{V}|/\lambda$, is obtained by knowing the transmission function of the molecular filter. Normalizing the filtered signal by the unfiltered signal removes the effects due to particle size distribution, particle number density distributions, optical effects, etc.

Figure 3 shows a schematic of a molecular filter profile that makes this measurement possible. The laser frequency is tuned so that its

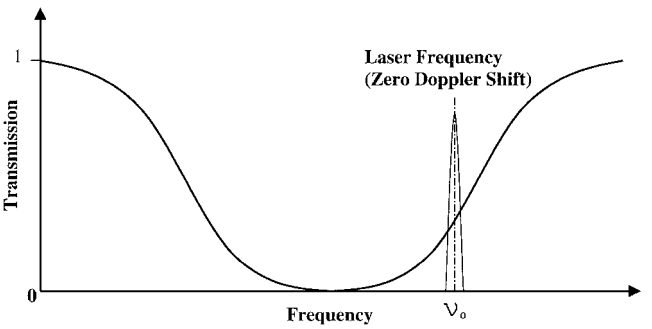

Fig. 3 Schematic of a molecular filter profile used with the PDV technique to measure the Doppler shift.

frequency is, in general, in the midpoint of the transition edge in between the maximum absorption and maximum transmission of the filter. With this arrangement, the molecular filter transmission is directly related to the Doppler shift or the flow velocity component in the $(\boldsymbol{s}-\boldsymbol{o})$ direction. With the Lorentz or pressure broadening technique, the slope of the transitional edges of the filter can be tailored to the dynamic range of expected velocity in the flow.[9–12,17–19] Obviously, to measure all three components of velocity, one must have a setup with three detectors that observe the scattering from three different directions. Again, this is similar to an LDV system in which a pair of laser beams and a detector are used for each component of the velocity vector. Issues associated with different components will be discussed, starting with the molecular filter.

Molecular Absorption Filter

In the PDV measurements, one is interested in measuring the Doppler shift of light scattered by the particles/molecules in the flow on the intersection plane of a laser sheet and the flowfield of interest. Molecular filters that possess features with a sharp edge and a smooth transition between their minimum and maximum transmission are very attractive for Doppler shift measurements. Shimizu et al.[52,53] were the first to discuss the use of an atomic or a molecular filter for frequency discrimination in atmospheric measurements using light detection and ranging technique. In fact, Shimizu et al.[52]

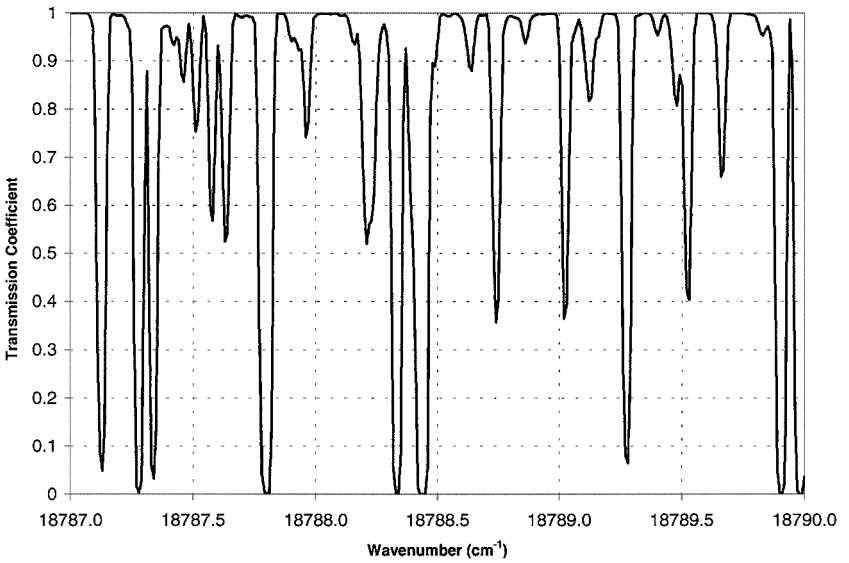

Fig. 4 Theoretical iodine absorption band around 18,788.45-cm^{-1} line used in the PDV technique.

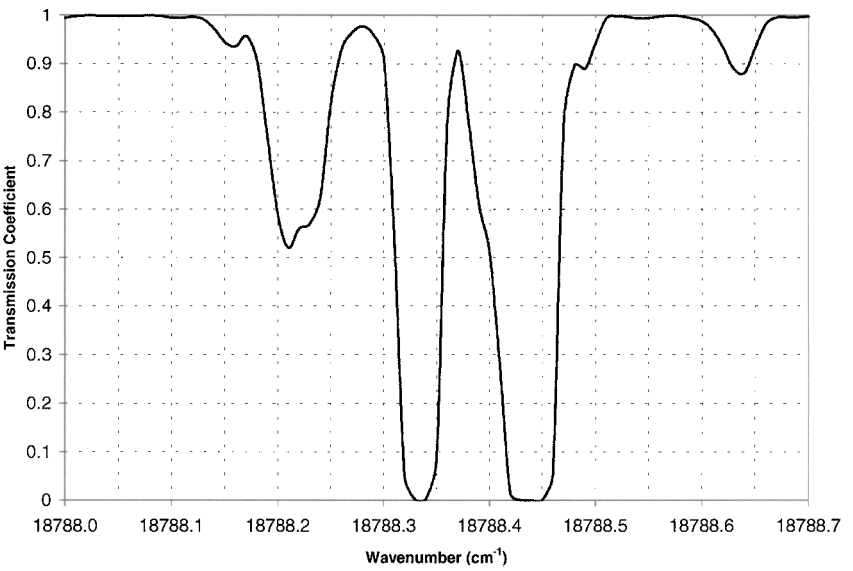

Fig. 5 Two theoretical iodine absorption lines in the vicinity of the second harmonic of the Nd:YAG (532-nm) line.

used an iodine molecular filter to remove the narrow linewidth scattering from aerosol to recover the Rayleigh scattering signal, which has a temperature-dependent line shape, from air molecules. Komine et al.[7] and Meyer and Komine[8] used an iodine molecular filter for velocity measurement in the DGV technique. Around the same time, Miles and Lempert[54] and Miles et al.[55,56] used an I_2 molecular filter with Rayleigh scattering to demonstrate the feasibility of measuring mean velocity, density, and temperature in high-speed flows. This was followed by some more work on the further understanding of iodine filter characteristics,[57,58] the development of other molecular or atomic filters,[59–62] the use of molecular filters with either Rayleigh or Mie scattering for background suppression in high-speed flow visualizations,[63–65] and the simultaneous, single-point measurements of velocity, density, and temperature in high-speed flows.[66,67]

The most widely used molecular filter to date is the I_2 filter. This filter has several attractive characteristics. It has strong absorption features in the visible range, especially around the second harmonic (532 nm) of the widely available and used Nd:YAG laser. Several of these features have strong absorption followed by a nearly full transmission, with a sharp smoothly and monotonically varying edge in between, over a frequency range of 1 GHz. This is ideal for fluid dynamics measurements. Forkey[68] has discussed these issues in detail and has provided a computational model and an accompanying computer code to calculate the absorption profiles of iodine in the visible light range, to identify the spectrally isolated lines, and to determine their sensitivity and dependence on the filter cell vapor pressure. Figure 4 shows the predicted absorption profiles using Forkey's code around 532 nm and within the tuning range of a typical Nd:YAG laser for a filter cell of 10 cm length L, the cell temperature T_{cell} of 85°C, and the iodine partial pressure in the cell, P_{I2}, of 0.46 torr. To calculate the iodine absorption profiles, Forkey used only the transitions from X to B, but ignored the background absorption due to the $X(^1\Sigma_g^+)$ to $^1\Pi_{1u}$ transitions. Therefore, his model correctly predicts the location, shape, and strength of the discrete absorption features, but overpredicts the maximum transmission and underpredicts the maximum absorption. Because the absorption profile used in the PDV technique is obtained experimentally, Forkey's code provides an excellent guide in the selection of the absorption lines, as well as a tool for a quick check of the experimental profiles. Figure 5 is a portion of Fig. 4 focused around a line (18,788.45 cm^{-1}) that is well-isolated on one side and has widely been used in the PDV applications.

Figure 6 shows a schematic of a molecular filter that is a cylindrical glass cell that contains the molecule of interest, mainly iodine, in vapor form. The diameter and the length of the cell are on the order

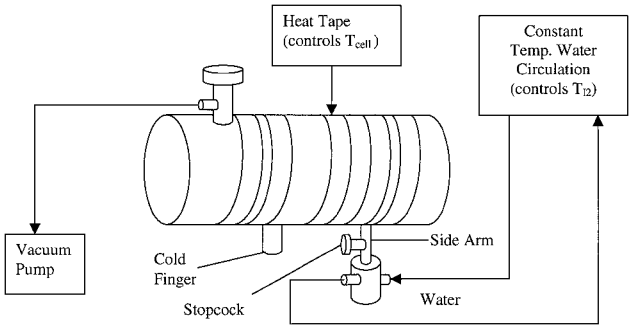

Fig. 6 Schematic of an iodine filter used in PDV.

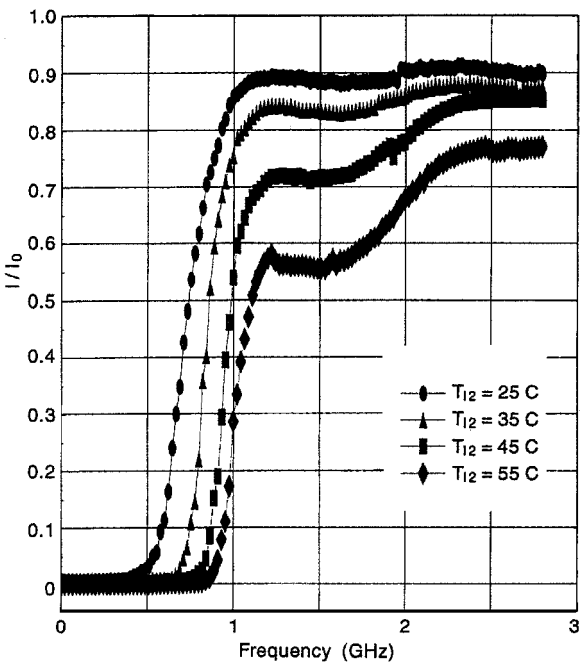

Fig. 7 Experimental Doppler-broadened filter profiles for different side arm temperatures.

of several centimeters. The cell is capped by optical quality glass windows at both ends. Three main features of the cell include 1) a vacuum port to evacuate the cell, and also to introduce a foreign inert gas into the cell in the case of a Lorentz-broadened filter, 2) a side arm with a stopcock valve and wrapped around with a water jacket to control the iodine partial pressure in the cell, and 3) a cold finger to crystalize the iodine content of the cell in the case of the pressure-broadened filter, in the filter preparation phase. The cell is wrapped with a heat tape to keep the cell temperature T_{cell} high enough (on the order of 100°C) to ensure that the iodine vapor in the cell would not crystalize in contact with the cell walls and, especially, the cell windows. The filter profile is sensitive to the side arm temperature that controls the iodine partial pressure. In Fig. 6, the stopcock valve just above the side arm water jack is closed after the filter has been prepared to trap all of the excess iodine in the side arm and the desired amount of iodine in the cell. Using this type of cell, Forkey[68] and Clancy[69] have shown that the filter profiles are insensitive to the cell temperature. However, if the excess iodine is not trapped in the side arm, the side arm temperature must be tightly controlled.[14,31] There are two types of filters: Doppler-broadened filter, in which the cell contains iodine vapor only, and the Lorentz-broadened filter, in which the cell contains an inert gas such as nitrogen in addition to the iodine vapor. These filters will be discussed next.

Doppler-broadened filters. The profile in this kind of filter is controlled by the partial pressure of iodine in the cell and the length of the cell. Figure 7 shows the experimental filter profiles[9,10] for the absorption line between 18,788.3 and 18,788.5 cm^{-1} (see Figs. 4 and 5) for several side arm temperatures and for a filter length of 10 cm and a cell temperature of 85°C. The side arm temperature T_{I2} of the cell determines the iodine partial pressure in the cell. Equation (2) gives the relation between T_{I2} and the iodine partial pressure in the cell, P_{I2} (Refs. 54 and 70):

$$\log_{10}(P_{I2}) = 9.75715 - \frac{2867.028}{254.180 + T_{I2}} \qquad (2)$$

The pressure and temperature in Eq. (2) are in torr and degrees Celsius, respectively. The iodine vapor pressure changes from 0.3 to 3.0 torr for the side arm temperatures given in Fig. 7. To set the iodine partial pressure in the cell, the cell is purged with an inert gas, such as nitrogen, to remove any moisture that might be present in the air and chemically react with the iodine, and then some iodine crystals are placed in the cell. Finally, the cell is evacuated to a low pressure (~0.1 torr), and the temperature of the side arm, T_{I2}, the coldest point of the cell, is established by running temperature controlled water through the water jacket. The water jacket temperature determines the side arm temperature and thus the partial pressure of the iodine in the cell according to Eq. (2). At equilibrium, the stopcock valve on the side arm is closed to trap the remaining iodine crystals. This fixes the iodine partial pressure and, thus, the filter profile. As shown in Fig. 7, the filter profile is sensitive to the filter side arm temperature or the iodine vapor pressure. Therefore, any temperature changes, in the absence of the stopcock valve or a tight control of the side arm temperature, will change the filter profile and, thus, will result in erroneous velocity measurements.

Doppler-broadened filters are ideal for the background removal or suppression in flow visualization applications in a wind tunnel, where the signal from the flow is overwhelmed by the background scattering from wind-tunnel walls and windows and the test model surfaces.[63–65] In such a case, the laser is tuned to the end of the maximum absorption and the beginning of the transition toward the maximum transmission in order to remove the strong zero Doppler-shifted background signal. The sharp transition in such a filter allows the transmission of a much weaker signal from the scatterers in the flow, due to its Doppler shift, even though it might be small. However, when such a filter is used in the PDV technique, it limits the dynamic range of the velocity that can be measured in a high-speed, highly turbulent flow in which even flow reversal might be encountered.

Iodine filters with the minimum transmission level as low as 10^{-3} are called optically thick profiles.[68] In fact, Seasholtz and Buggele[58] have shown that this minimum transmission level could be even lower by proper treatment of the Nd:YAG laser frequency around the 532-nm wavelength. By the increase of T_{I2} beyond 60°C or by the choice of some other absorption features, the minimum transmission could be raised significantly. Such filters are called optically thin filters, which have more gradual transmission slope between the minimum and maximum transmission and have been used by some researchers, due to their simplicity. Note that by switching from the optically thick filter to the optically thin filter, the slope of the transitional region of the filter between the minimum and maximum transmission is reduced without any gain in the dynamic range of the velocity that can be measured. The dynamic range of the velocity that can be measured with PDV using optically thin filters can be increased, to some degree, by the use of cell conditions that optimize the filter sensitivity. However, for a substantial increase in the dynamic range, an optically thick filter that is pressure broadened must be used. These filters will be discussed next.

Lorentz- or pressure-broadened filters. The Doppler-broadened filters that were just discussed have a very sharp transition between the maximum absorption and the maximum transmission. To increase the dynamic range of the velocity that can be measured by PDV, Elliott et al.[9,10] used a Lorentz- or pressure-broadened filter. In such a filter, the addition of an inert gas such as nitrogen into the filter cell causes the collision of nitrogen and iodine molecules, which changes the profile of the filter in such a way that the transition between the maximum absorption and transmission is much more gradual. The slope of this transition can be changed by changing the number density of nitrogen in the filter cell, thus enabling the experimenter to tailor the filter to the dynamic range of the velocity of interest. Figure 8 shows the experimental filter profiles for the absorption line between 18,788.3 and 18,788.5 cm^{-1} (see

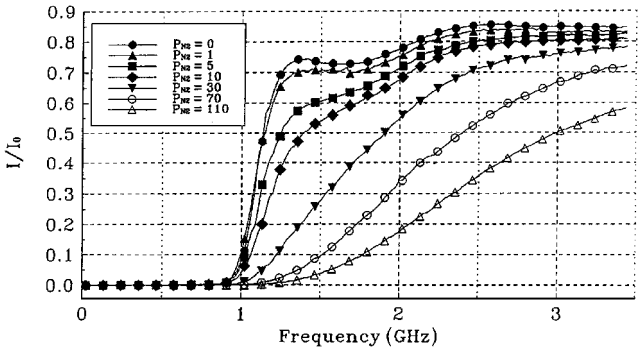

Fig. 8 Experimental pressure-broadened filter profiles for different nitrogen partial pressures.

Figs. 4 and 5) for nitrogen partial pressure from 0 to 110 torr, for $T_{12} = 30°C$, $T_{cell} = 85°C$, and $L = 10$ cm (Refs. 9 and 10). As can be seen, the dynamic range of the velocity that can be measured using a pressure-broadened filter can be increased by a factor of over five. Obviously, the increased dynamic range comes at the price of a reduced sensitivity to Doppler shift. To add nitrogen to a temperature-broadened filter, the cold finger is immersed in an acetone–dry ice slurry to drive all of the iodine vapor to the crystalline state. Then, nitrogen is added via the vacuum port. After the introduction of an appropriate level of nitrogen, the vacuum port is sealed, the acetone–dry ice slurry is removed from the cold finger, and the filter is allowed to return to its equilibrium state.

Light Source

In the PDV technique, the Doppler shift of light scattered by the particles in the flow is measured with respect to the frequency of the laser. Some of the central characteristics of the light source for the PDV application are 1) it must have a narrow linewidth, 2) it must be tunable on the order of several gigahertz, and 3) it must operate in the frequency range that is convenient for the use of iodine filters and charge-coupled device (CCD) cameras. In addition, the laser must be readily available, economical, and robust. Both the Nd:YAG laser and the argon laser meet these criteria. Even though both the second harmonic (532 nm) of the Nd:YAG and the green line (514.5) of the argon laser have been used with PDV, the discussion will focus on the Nd:YAG laser. The main interest in the PDV technique is in its capability for planar multiple-component, instantaneous velocity measurements, which are only possible by using a pulsed Nd:YAG laser. For those interested in the argon laser use in PDV and, hence, time-averaged velocity measurements, there are several publications.[8,25,29,71]

The standard YAG lasers operating at 532 nm have a linewidth on the order of at least several gigahertz, which is too wide for the PDV application in which the molecular filter edge frequency span is less than 1 GHz. However, using a continuous wave YAG laser with a very narrow linewidth (approximately kilohertz) as an injection seeder, the linewidth of the pulsed YAG lasers can be narrowed down to approximately 100 MHz, which is adequate for the PDV application. The addition of an injection seeder also provides tunability in the range of several gigahertz to these lasers. Unfortunately, it is known that these lasers have a long-term drift and also pulse-to-pulse variations in both frequency and power. The variation in the laser power is removed when the filtered signal is normalized with the unfiltered signal; therefore, it does not pose a problem. The problem with the frequency drift and fluctuations can be remedied experimentally by taking a very small portion of the laser beam, splitting it into two, then focusing the parts onto two fast-response photodetectors after passing one of the beams through another iodine filter.[13–22,31] With this simple system, one can monitor the changes in the laser frequency and incorporate them into the Doppler shift calculations. It has been shown[20,22] that, with a system similar to the one just described, that uses fast photodetectors of better than 1-ns response time and an integrator, one can measure the laser frequency variations within 2 MHz.

When a laser sheet is formed, another area of concern is how consistent the light frequency across the laser sheet is. Obviously, any variations in the frequency across the laser sheet would contribute to the error in the velocity measurements. Forkey[68] and Forkey et al.[57] noticed a frequency variations of about 100 MHz across the laser beam. The source of this variation is not clear. However, Clancy[69] and Clancy et al.[18,19] showed that when they used only the middle portion of the sheet (approximately 60%), the variation of the frequency across the sheet dropped to about 4 MHz.

Absorption Filter Spectral Transmission Function

The absorption filters and the Nd:YAG laser used in the PDV technique have been discussed. After the preparation of a filter, the actual transmission profile of the filter must be obtained before experimental data can be taken. The process involves 1) setting up the laser sheet and cameras for the actual experiment (Figs. 2 and 9), 2) placing a glass container that contains particles such as powdered milk dissolved in water in the test section of the experiment,[15,17,19] 3) passing the laser sheet through the glass container, 4) collecting the scattered light by each camera (both filtered and unfiltered images), and 5) tuning the laser over the frequency range of interest, which covers the transition region of a line from maximum absorption to maximum transmission, about a gigahertz for a Doppler-broadened filter and could be a few gigahertz for a Lorentz-broadened filter. The profile obtained by plotting the ratio of the filtered image intensity I to the unfiltered image intensity I_0, at each frequency, defines the spectral transmission function of that given filter. Such function is obtained for all of the filter. For a given I/I_0 in the actual experiment, the transmission function gives the Doppler shift, and Eq. (1) gives the component of velocity in the $(\boldsymbol{s}-\boldsymbol{o})$ direction.

PDV Configurations

In measuring the Doppler shift in the scattered light frequency, the scattered light is divided into two approximately equal intensity beams that are then focused side-by-side onto a single camera: one image directly and the other image after passing through an absorption filter (see Fig. 2). Normalizing the filtered image with the unfiltered image removes the effects of particle size and number density distributions, the fluctuations in the laser power from pulse-to-pulse, the optical effects, and the potential laser light polarization effects in the beam splitter used in this system. The main optical effects include the variations of CCD camera pixel gain, the spatial variations in transmission of the light collection optics and camera lens, and the transmission differences in the filtered and unfiltered path. To obtain both filtered and unfiltered images, initially, the scattered light at an angle was either divided by a beam splitter then put onto two separate cameras[7,8] or was directly received by two cameras.[9–12] In either case, a molecular filter was located in front of one of the cameras to obtain the filtered image. Lately, a splitter system has been used, as shown in Fig. 2, in which the scattered light at an angle is split in two by a beam splitter; after passing one of the beams through an absorption filter, the beams are focused side-by-side onto a single camera.[13–19] In addition to making the PDV system more compact and robust, this system makes the technique more economical by reducing the number of cameras from six to three for three-component measurements.

Figure 2 is a schematic of a PDV system to measure the Doppler shift. However, the purpose of the PDV technique is to obtain the velocity of the flow, not the Doppler shift. With the arrangement in Fig. 2, using the measured Doppler shift and Eq. (1), only the component of the flow velocity in the $(\boldsymbol{s}-\boldsymbol{o})$ direction with a magnitude of $|(\boldsymbol{s}-\boldsymbol{o})\cdot\boldsymbol{V}|/\lambda$ is obtained. One can obviously arrange to obtain a single component of the velocity in a given desirable direction by a setup similar to the one shown in Fig. 2. However, to obtain all three components of velocity, one has to either bring the laser sheet from three different directions or to observe the scattering from three different directions. The latter option is much simpler for three-component measurements and has recently been used by Clancy et al.[18,19] However, the first option has also been used recently for three-component mean velocity measurements in a low-speed flow by Roehle et al.[33]

Figure 9 is a typical PDV setup for three-component velocity measurements. In this configuration, the bulk flow is in the x direction

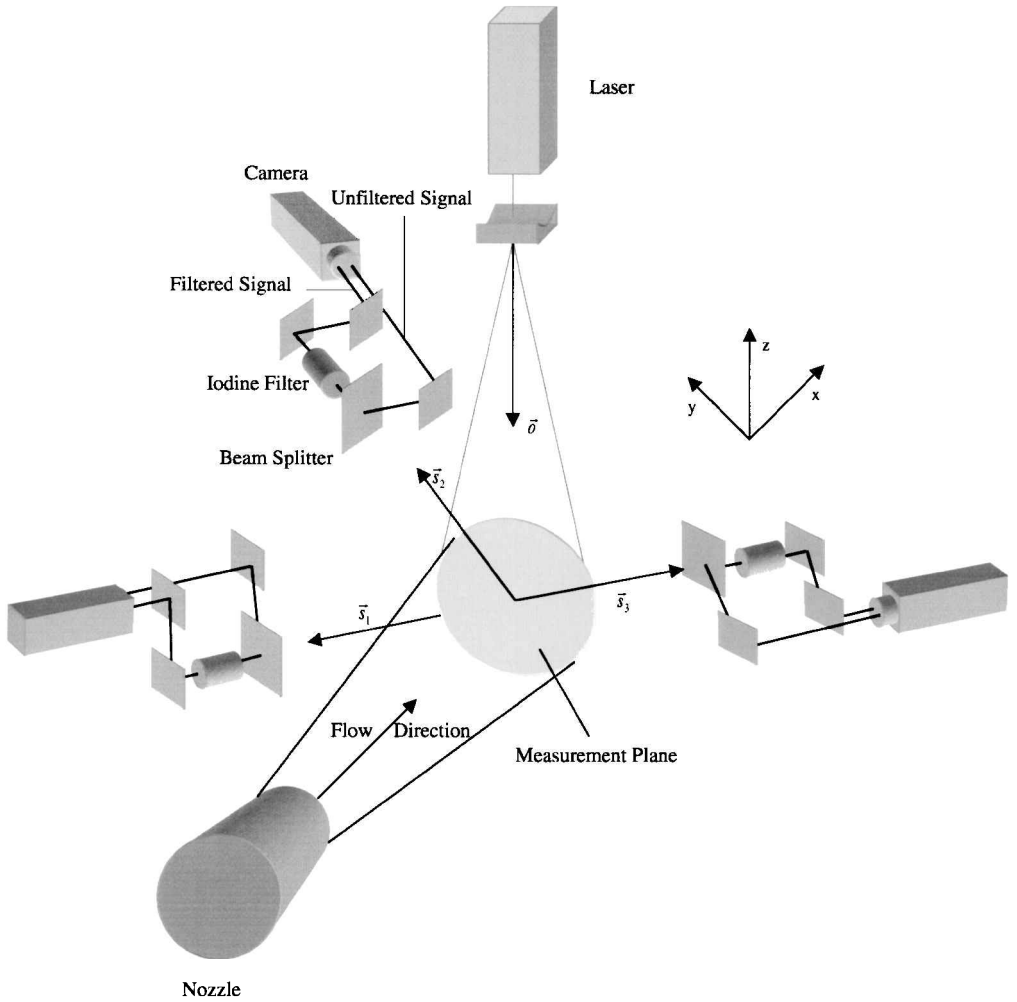

Fig. 9 Schematic of a three-camera-based, three-component PDV system.

(but the flow could be a three-dimensional flow that possesses all three components of velocity, V_x, V_y, and V_z), all of the cameras are in the x–y plane, and the laser sheet is normal to the x–y plane (in the y–z plane). A preliminary sensitivity analysis of the system shown in Fig. 9 indicated that the optimum setup of the system calls for the tilting of one of the cameras in the z direction and another in the negative z direction. The laser sheet could be in the x–y or y–z plane, depending on the application. As an example, take a high-speed jet flow in which the interest is in the passive control of the mixing and noise of the jet by imparting streamwise structures into the flow.[72] Using the laser sheet on the x–z plane, one can get detailed information on the Kelvin–Helmholz type of structures in the flow, whereas using the laser on the y–z plane will show the details of the imparted streamwise structures in the flow. One of the attractive attributes of PDV, in comparison with PIV, is that it is capable of obtaining planar measurements with similar spatial resolution and accuracy whether the laser sheet is aligned with the x–z plane (a plane parallel to the bulk motion direction) or with the y–z plane (a plane normal to the bulk flow direction), provided that the necessary optical access is available.

Image Registration and Matching

In the PDV technique, there are two pixel-by-pixel image matching steps: The first one is in the calculation of the Doppler shift for each viewing angle shown in Fig. 9, and the second one is in the calculation of the velocity components from these Doppler shifts. The Doppler shift for each observation angle Δf_d is calculated using Eq. (1). The equations to calculate the velocity components from the three Doppler shifts for a configuration similar to the one shown in Fig. 9 are[69]

$$\Delta f_{d1} = [V_x \cos(\alpha) + V_y \sin(\alpha) + V_z]/\lambda \quad (3)$$

$$\Delta f_{d2} = [V_x \cos(\beta) + V_y \sin(\beta) + V_z]/\lambda \quad (4)$$

$$\Delta f_{d3} = [V_x \cos(\gamma) + V_y \sin(\gamma) + V_z]/\lambda \quad (5)$$

In these equations, α, β, and γ are the angles that the observation unit vectors $\boldsymbol{s}_1$, $\boldsymbol{s}_2$, and $\boldsymbol{s}_3$ make with the x axis, respectively. Initially, two cameras were used to record a pair of filtered and unfiltered images.[7–12] Lately, a system has been used (Fig. 2) that records both filtered and unfiltered images side-by-side on a single camera.[13–19] In either setup, the filtered images must be normalized pixel-by-pixel by the unfiltered image to obtain the Doppler shift. Smith et al.,[15] Smith,[16] and Clancy et al.[18,19] have shown that this pixel-to-pixel matching plays an important role in the accuracy of PDV, and the process must be carried out to subpixel precision for accurate velocity measurements. In a recent work, Arnette et al.[23] showed that one could potentially eliminate the problems associated with this image registration by using a two-color illumination and a color camera scheme. For this purpose, they used 532- and 618-nm lines from a Nd:YAG laser and a YAG pumped dye laser and an iodine filter in resonant interaction with the 532-nm line. More work is required to delineate various issues in using color cameras for PDV.

After measuring all three components of the Doppler shift (Δf_{d1}, Δf_{d2}, and Δf_{d3}) by using a setup such as the one shown in Fig. 9, Eqs. (3–5) must be solved simultaneously to determine all three components of the velocity (V_x, V_y, and V_z). Obviously, the normalized images must be matched pixel-to-pixel among all three cameras.

To obtain an accurate pixel matching, the image of either a grid of white dots on a black background (when cameras are located on one side of the grid plane) or on a transparent background (when cameras are located on both sides of the grid plane) located at the measurement plane (the cross section of the laser sheet and the flow) has been used.[18,19,25–27,30,31] Clancy et al.[18,19] obtained the image of

the grid under normal room lighting and used it as a reference image. They first determined the centroid of each dot on both filtered and unfiltered images, then used the necessary shifts in two dimensions to match the dots. Finally, they used these shifts to calculate the nongrid points using a two-dimensional bilinear interpolation. This technique was used to first match the filtered and unfiltered images in the Doppler shift calculations, then to match the pixels in all two or three cameras for velocity calculations.

When a filtered image is normalized with its counterpart unfiltered image, one expects this process to remove the light intensity variations in the filtered image caused by anything other than the Doppler shift. The hidden assumption here is that all of the optics used to split the scattering signal are put onto two different cameras or a different part of a camera and this does not affect the images and the gain on two cameras and across a camera is uniform. Depending on the setup, this assumption could obviously introduce major errors in the PDV measurements if it is not properly treated. To ensure that all of these potential light intensity variations are removed, a calibration is performed. It is found that the best procedure for calibration is to use the exact setup that is used in flow measurement, except the laser is tuned for the maximum transmission.[11,12,18,19] Then several laser power levels are used to obtain filtered and unfiltered images or flatfield images. Note that the camera gain should be kept at the same level as when the velocity data were taken. Because the filter is ineffective in this setup and because the optical effects are linear, Clancy et al.[18] showed that one obtains a linear relation between the filtered and unfiltered intensities. The slope of this line is used in the normalization process to remove all of the optical effects of the setup.

Scattering Particles

PDV, similar to LDV and PIV, is a particle-based velocimetry technique. There are several issues associated with the seed particles in these techniques. These issues are 1) the availability, environmental impact, cost, generation, and introduction of particles into the flow; 2) the statistical biases; 3) the particles' response to the dynamics of the flow; and 4) the spatial resolution. These issues will be briefly discussed. Obviously, the seed particles must be readily available, and they must be environmentally benign. They also must be economical and easy to produce and to introduce into the flow. These are common issues in all three techniques and have received considerable attention over the past two decades.[73–78] In LDV and PIV applications, polydisperse (nonuniform distribution of size) particles of various kinds have been used. For example, liquid particles such as vegetable oil and silicone oil have been atomized and used,[46,76] solid particles such as alumina have been directly introduced into the flow,[74] particles such as titanium dioxide have been generated by mixing of titanium tetrachloride vapor and moist air in the flow,[77] or particles have been generated by combustion processes,[78] just to name a few. Also monodisperse (uniform distribution of size) particles such polystyrene latex suspended in a volatile liquid have been used.[73] When solid particles are used, their uniform dispersion is a challenging task. There are some recent promising developments in this area.[16,79,80]

Most of the issues discussed are common among PDV, PIV, and LDV techniques. However, both PIV and LDV have constraints in terms of the upper limit for the number density of the particles in the flow. The particles in between two successive images in PIV must be correlated. This puts certain restrictions on the number density of particles used so that the individual particles are resolved on the CCD.[37] In LDV, fringe crossing of more than one particle at a time causes problem with the detection system. This problem also restricts the number density of particles. On the other hand, there is no such restriction on the particle number density in PDV. Note that with a high particle number density, one can use much smaller particles because the signal received by a detector from particles in the measurement volume is accumulative. Therefore, smaller particles with high particle number density could be used with the PDV technique. This makes PDV superior in terms of particle flow dynamics fidelity and also in achieving higher spatial resolution.

Generating smaller particles in large quantity is obviously much more challenging. Various kinds of particles have been used with PDV. One of the techniques that can generate very small particles ($\sim$50–100 nm in diameter) of almost continuous phase is generating particles by vaporization/condensation processes, which has been carried out in high-speed flows.[9–12,15,17–20] This technique is not suitable in low-speed and high-temperature applications. Therefore, techniques such as those recently developed by Wernet and Wernet[79] and Smith,[16] for example, could be used to disperse solid particles of a fraction of a micron in diameter in such cases.

There are statistical uncertainties and biases associated with techniques such as LDV, PIV, and PDV. The most obvious statistical uncertainties are those associated with the image sample size that can easily be overcome. For example, Clancy et al.[18,19] showed that by using about 150 images, the statistical uncertainties in the mean velocity was relatively small. However, the sample size must be much higher to significantly drop the statistical uncertainties.[42] For higher-order statistics, obviously, the number of images required for statistics to converge would be even higher. On the other hand, there are statistical biases that are not well understood, and there does not seem to be an effective way to treat them. One such bias, which is common in all seed particle scatterer-based techniques such as LDV, PIV, and PDV, is the bias due to the nonuniform seeding. One can easily understand this bias by looking at the application of one of these techniques in a two-stream flow where only the high-speed stream is seeded. Assume that the measurement volume is located in the mixing region of the flow. Because only the high-speed stream is seeded and because the measurements are from the seed particles, then if a particle carrying structure that was originated in the high-speed stream is located in the mixing region at the time of measurement, the velocities associated with that structure will be imaged. These velocities, of the flow elements coming from the high-speed side, will be much more energetic and dynamic. On the other hand, if a structure that was originated from the low-speed stream is located in the mixing region at the time of the measurement, the velocities associated with that structure, which most probably are lower and less dynamic, will not be imaged because the structure does not contain seed particles. If one uses a number of these images to obtain statistical information, the data will be biased toward the characteristics of the high-speed flow. As was mentioned, this is not a well-understood bias, and there is no treatment for it other than making an attempt to have uniform particle number density in all regions of the flow.

Another problem common to all of the seed-particle-based optical diagnostics is that the seed particles have inertia that would influence their flow tracking.[81,82] Obviously, this problem is more acute in high-speed flows, which possess higher frequency fluctuations. The Stokes number of the particles in the flow determines the range of turbulence fluctuation frequencies in the flow that the particles would be able to respond to. The Stokes number St is defined as the ratio of the particle aerodynamic response time ($\tau_p = \rho_p d_p^2 / 18\mu$) to the flow timescale τ_f, that is, $\mathrm{St} = \tau_p / \tau_f$, where ρ_p is the particle density, d_p is the particle diameter, and μ is the viscosity of the fluid.[83] Samimy and Lele[84] have shown that in free shear flows, for example, the Stokes number of the particles used for flow diagnostics must be smaller than 0.05 for the particles to follow energy containing large turbulence structures in the flow. For the particles to follow smaller scale structures, the Stokes number must be much smaller than 0.05. The key issue here is that for a given particle and flow combination, the Stokes number is proportional to the square of the particle diameter. By decreasing particle diameter from 0.5 to 0.05 μm (50 nm), for example, the Stokes number drops by two orders of magnitude. Another issue is the response of particles to steep gradients in the flow. This issue has been investigated by passing particles through a steep but known gradient, such as one setup by a shock wave. It has been shown that the distance for a particle to relax back to the flow velocity changes asymptotically with particle diameter.[76] From this argument, it is clear that PDV, which can use smaller particles, has an advantage over PIV, especially in high-speed turbulent flows in which the dynamic range of turbulence fluctuations frequency is very high.

The last issue concerning the seed particles is their effect on the spatial resolution of the measurements. The PIV technique relies on the particle transit time in between two successive images to measure the particle velocity. One has to compromise between the spatial

resolution of the measurement, which demands very short particle travel in between two images, and the accuracy of the measurement of the distance, which requires larger travel distance in between images, for improved accuracy. This problem becomes more acute in three-component velocity measurements using PIV. Obviously, this issue is related to the nature of the technique and not on the seed particles. On the other hand, PDV is based on the Doppler shift of the scatter light from a single laser pulse. Therefore, it offers a higher spatial resolution. As was discussed earlier, PIV has to use larger particles with lower particle number density, in comparison with PDV. Similar to the number of grid points in the numerical simulation that determines the extent of the turbulence scales that a simulation can capture, the much larger number density of particles used in PDV directly translates into the higher spatial resolution for PDV.

Spatial Resolution

As was discussed in the Introduction, for a laboratory-scale 25-mm-diam supersonic jet of Reynolds number 10^6, the range of turbulence scales spans from approximately 1 μm to 25 mm. With the current technology, developing an optical measurement technique that can simultaneously cover this range of scales is not achievable. Having said that, it is instructive to explore the limits of planar optical techniques, in general, and to determine the range of scales that can be measured in such a facility. The main limitation arises from the laser light being an electromagnetic wave and being subjected to the diffraction limits. Diffraction limits the spatial resolution of all planar measurements in three ways: The first effect deals with the recording system/camera lens, and the other two diffraction effects are concerned with the light sheet formation. Diffraction limits the minimum resolvable in-plane separation between two discrete objects, which is basically the smallest scale that can be measured by the image recording system. This is called the Rayleigh criterion and is determined by[85]

$$\text{Res} = 1.22\lambda f_I / D_I \tag{6}$$

where Res is the resolution of the imaging system, λ is the wavelength of the light being used, and f_I and D_I are the focal length and diameter of the imaging lens. Next, diffraction puts a lower limit on the thickness of the laser sheet, t, that can be generated. This laser sheet thickness determines the out-of-plane resolution of the technique. This laser sheet thickness, or beam waist, is given by[86]

$$t = 2\lambda f_F / D_{e^{-2}} \tag{7}$$

where $D_{e^{-2}}$ is the diameter of the laser beam before the focusing lens and f_F is the focal length of the focusing lens. Diffraction will also cause the focused light sheet to diverge away from the minimum waist thickness t. The Rayleigh range ℓ_t is the distance on either side of the beam waist that the thickness will increase by about 40% and is given by[86]

$$\ell_t = \pi t^2 / \lambda \tag{8}$$

In the field of view of $2\ell_t \times 2\ell_t$ the laser sheet thickness would increase from t (at the beam waist) to $1.4t$ toward the edges of the sheet. This obviously would limit the out-of-plane resolution of the technique. From Eqs. (7) and (8), it is obvious that decreasing f_F and increasing $D_{e^{-2}}$ would improve the spatial resolution, but would also decrease the field of view. Therefore, for a given case with specified constraints, one can optimize the system for spatial resolution.

Let us assume that the PDV resolution is diffraction limited. We will show shortly that this is probably the case. For PDV to be able to measure the largest turbulence scale in the jet flow as discussed earlier, the extent of the laser sheet must be at least the same as the largest turbulence scale (25 mm), which gives $\ell_t = 12.5$ mm. For a typical pulsed Nd:YAG laser, λ is 532 nm and $D_{e^{-2}}$ is approximately 8 mm. Equations (7) and (8) give $t = 46$ μm and $f_F = 34.6$ cm. Therefore, the minimum and maximum laser sheet thickness would be 46 and 65 μm. Therefore, the out-of-plane spatial resolution of the technique would be limited to the maximum laser sheet thickness of 65 μm within the field of view. If we take $f_I = 50$ cm and $D_I =$ 5 cm, Eq. (6) gives a minimum resolution of the optical system of approximately 6.5 μm. However, assuming we use a 1000×1000 pixel CCD camera to image the 25×25 mm field of view, then the limiting in-plane spatial resolution on the CCD is 25 μm, which is approximately the size of a pixel in a standard scientific-grade CCD camera. Therefore, the laser sheet thickness establishes the minimum turbulence scale that can be measured in this given facility, which is between 46 and 65 μm, if the technique is diffraction limited.

As will be discussed in detail later, the speckle noise could affect the spatial resolution of PDV. This stems from the use of a coherent light in PDV. When coherent light is scattered by a nonuniform distribution of particles, the detector receives light of nonuniform phase that interferes with itself and forms speckle noise that is superimposed on the image. Depending on the speckle noise level, a PDV image could appear grainy. Using a small f-number lens and/or a CCD array with large pixel size could reduce the speckle noise.[87] McKenzie[14] has shown that binning of several adjacent pixels is necessary to overcome sampling errors that are inherent in the normalizing of CCD array images. The out-of-plane spatial resolution of diffraction limited PDV, calculated earlier, is approximately the size of 3 pixels in a CCD camera. It looks as if binning of several adjacent pixels would take care of the speckle noise and sampling error; it would also keep the spatial resolution within the diffraction limits. As was discussed, the CCD imaging resolution for a 1000×1000 pixel sensor was 25 μm, which when binned together in a 3×3 area produces a limiting spatial resolution of approximately 75 μm. The resolution could be higher or lower depending on the application.

The theoretical spatial resolution of PDV determined earlier could be reduced to some degree due to the nature of the technique, in which at least one of the cameras must view the measurement volume in an oblique angle (Fig. 9). The oblique view results in perspective distortion in the recorded image. Although calibration grids and image warping are used to remove the perspective distortion, the raw image data are still recorded with this distortion. The main effect of the perspective distortion is the change in magnification and the concomitant change in spatial resolution across the image plane. To first order, the magnification M in an oblique viewing optical system is

$$M = \ell_i / (\ell_0 + \chi \sin\phi) \tag{9}$$

where ℓ_i is the distance from the imaging lens to the CCD detector, ℓ_0 is the distance from the measurement plane to the lens, ϕ is the angle between the camera and the normal to the illumination plane, and χ is the coordinate on the measurement plane with its origin centered at the center of the plane. Hence, it can be seen that the magnification of the optical system could be smaller for positive values of χ (moving away from the camera system) and that the magnification is larger for negative values of χ (moving closer to the camera system). The variation in magnification is also dependent on the viewing angle, decreasing for larger viewing angles. The portion of the image closest to the camera has the largest magnification and spans the full height of the CCD sensor. However, the portion of the image farthest from the camera has the smallest magnification and does not span the full height of the sensor. This could degrade the spatial resolution of the PDV measurements. The relative distance between the camera and the measurement plane is also important. For $\ell_0 \gg \chi$, which is the case in general, the magnification will be nearly uniform. For example, the horizontal variation in vertical magnification for the 25-mm measurement plane discussed earlier (χ ranging from -12.5 to $+12.5$ mm), imaged at a distance of $\ell_0 = 346$ mm, lens to camera distance of $\ell_i = 50$ mm, and a viewing angle of 30 deg yields a 3.6% variation in the magnification factor M. Hence, at one end of the CCD sensor, the image spans all of the pixels, whereas at the other end, the image spans only 96.4% of the pixels. Obviously, the oblique viewing does not cause a major problem in this example. However, the perspective distortion from one or more cameras with oblique views in a three-component PDV system should be checked and accounted for and could reduce the overall spatial resolution of PDV.

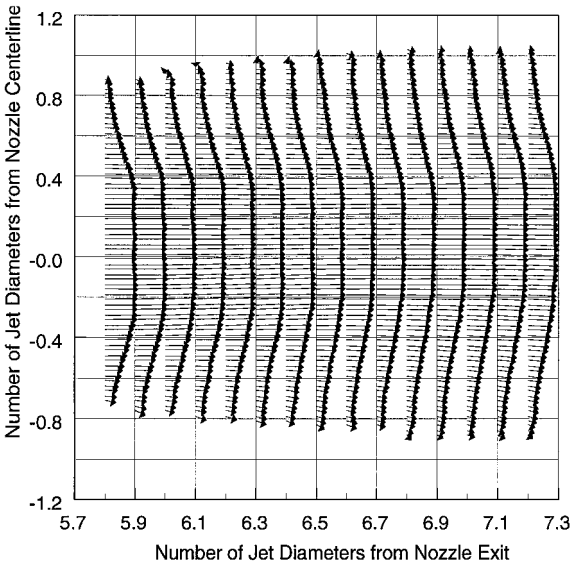

Fig. 10 Mean velocity vector in the x–z plane of a Mach 2 axisymmetric jet (the centerline velocity is approximately 480 m/s); V_y was measured but is not shown.

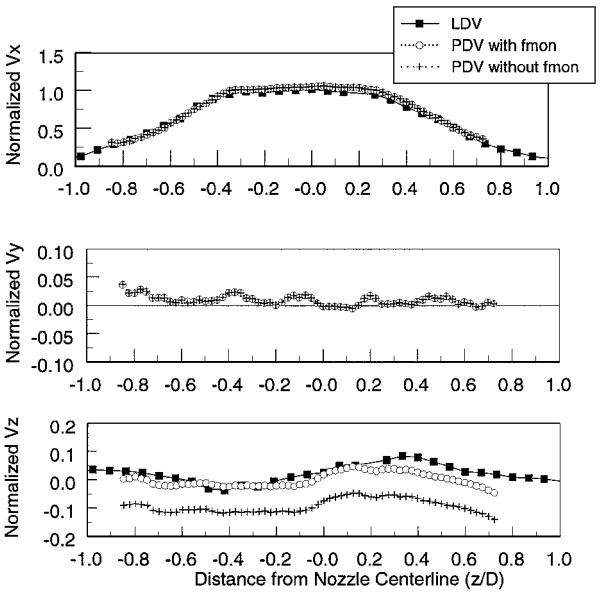

Fig. 11 Comparison of LDV and PDV mean velocity profiles of a Mach 2 jet at 6 jet diameters downstream of the jet exit; PDV results obtained both with and without using a frequency monitoring system.

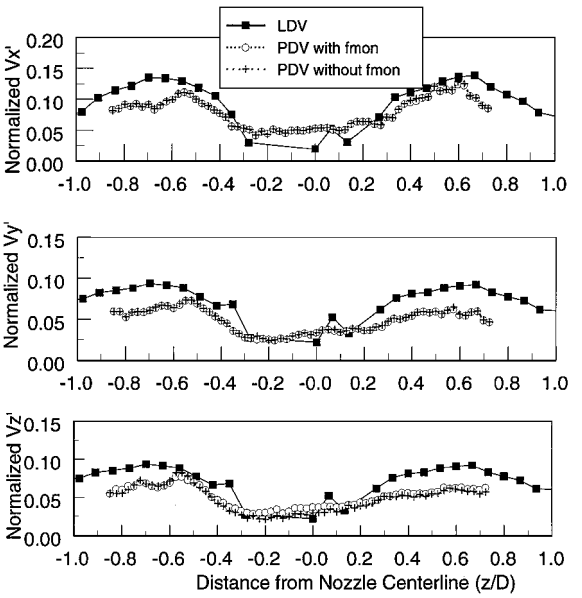

Fig. 12 Comparison of LDV and PDV turbulence intensity profiles of a Mach 2 jet at 6 jet diameters downstream of the jet exit; PDV results obtained both with and without using a frequency monitoring system.

Sample PDV Results

High-speed flow measurements using PDV or DGV have been made in several laboratories in recent years. The flows include mixing layers,[9,10] boundary layers,[11,12] jets,[15–19,21] and transverse jet in a crossflow.[20] To show the capabilities of PDV in high-speed flows, some sample results in a supersonic jet obtained in the laboratory of the first author of this paper using a three-component PDV will be presented.[17,18,69] Figure 10 shows the mean velocity vectors for a Mach 2 freejet, with an exit diameter of 19 mm and the Reynold number of 2.1×10^6, from approximately 5.7 to 7.3 jet diameters downstream of the exit. The jet was fully expanded with a stagnation temperature of approximately 280 K. The results include only the x (the flow direction) and z components of the velocity. These measurements were obtained by using a split image system for each velocity component (Fig. 2) and three intensified CCD (ICCD) cameras for three-component measurements (Fig. 9). The setup is similar to the schematic shown in Fig. 9 with the laser sheet oriented in the streamwise direction (x–z plane) and contains the centerline of the jet. The angles for the three detectors with respect to the x direction (the angles that s_1, s_2, and s_3 make with x) were 63, 121, and −90 deg. The mean velocities and the turbulence intensities were calculated based on 251 images. Approximately half of the velocity vectors have been dropped to avoid the cluttering of Fig. 10. The results shown in Fig. 10 unquestionably indicate the planar capabilities of PDV, the extent of the detailed information it can provide, and typical dynamic range of velocity obtainable that spans from very low velocities in the mixing region to about 480 m/s at the center of the jet.

To determine the accuracy of the PDV results, they were compared with the results from a two-component LDV obtained in the same facility. Figures 11 and 12 show comparison of LDV and PDV results for both the mean velocities and the turbulence intensities at one x location, six jet diameters downstream of the jet exit. All of the mean velocities and turbulence intensities are normalized with the jet centerline velocity of approximately 480 m/s. The results show good agreement between PDV and LDV mean velocity and fair agreement between turbulence intensity results. The laser frequency fluctuations and methods to monitor them in the PDV measurements were discussed earlier. The results in Figs. 11 and 12 show how the monitoring of the laser frequency fluctuations and their incorporation into the calculations significantly affect the z component of the velocity but not the x component or the turbulence intensities. The reason for this is that the random fluctuations in the laser frequency average out in the calculation of the turbulence intensities. On the other hand, the mean velocities are obtained by using Eqs. (3–5), where the nature of the equations depends on the setup. Some velocity components are obtained by subtracting two Doppler shift components (such as the x and y component in this case). If there are any laser fluctuations from pulse-to-pulse, they affect both components in the same fashion, and thus, the effect nearly cancels out.[17–19,69]

Earlier it was discussed, under the subheading "Image Registration and Matching," that the filtered and unfiltered images (Fig. 2) and also images among the cameras (Fig. 9) must be matched pixel-by-pixel. Figure 13, for example, shows how, in a two-component PDV system used in a Mach 2 fully expanded axisymmetric jet at six jet diameters downstream of the exit, changing the matching accuracy from a subpixel (Fig. 13a) to pixel (Fig. 13b) adversely affects the results.[17]

Figure 14 shows the streamwise (x component) mean velocity map and both an instantaneous and the mean cross-stream velocity vectors (y and z components) at the jet cross section located three jet diameters downstream of the jet exit. The intensity to velocity conversion scale in Fig. 14a is in meters per second. The flow was an underexpanded jet from a converging nozzle with a jet Mach number

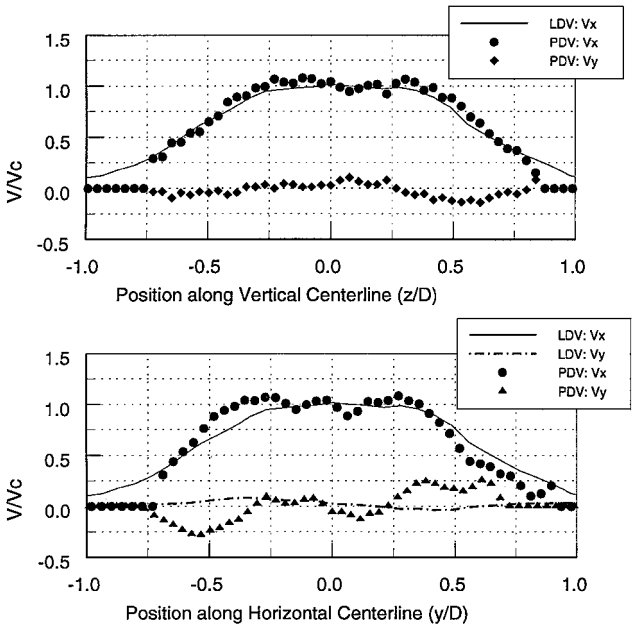

Fig. 13 Comparison of two-component PDV and LDV mean velocity results in a Mach 2 jet 6 jet diameters downstream of the jet; PDV results were obtained with subpixel (top) and with a pixel (bottom) image registration accuracy.

of 2 and with a single vortex generating tab attached to the nozzle exit.[69,88] The jet Mach number corresponds to a Mach number had the jet isentropically expanded to the ambient pressure. This kind of tab has been used to generate strong streamwise vortices in order to passively control the jet mixing and noise characteristics.[89–91] Again, the measurements were obtained by using a split image system that uses three ICCD cameras for three-component measurements. The setup is similar to the schematic shown in Fig. 9 with the laser sheet oriented normal to the streamwise direction of the jet (on the y–z plane). The angles for the three detectors with respect to the x direction were 32, 129, and −37 deg. Approximately 140 images were used to calculate the mean velocities.

In these experiments, the seed particles were generated when the moist ambient air was mixed with the cold and dry jet air. Therefore, the measurements were obtained only in the mixing region of the jet. Again the dynamic range of measured velocities is from very small velocities to about 500 m/s. The instantaneous (9-ns exposure time) image (Fig. 14b) shows a very intricate flow pattern that contains eddies of various sizes. These results show the capability of PDV for simultaneous instantaneous measurements of all three components of velocity on a plane normal to the bulk mean flow direction. Whereas similar measurements could potentially be obtained using PIV in low speed, the spatial resolution of the measurements would be much lower.[51,92–94]

In Fig. 14c, annotated vectors identify three sets of vortices. The existence of these vortices has been reported in low-speed flows,[91] but their existence has only been hypothesized in supersonic flows.[90] The first pair of vortices (HN and HP) are the horseshoe vortices generated by wrapping of the boundary-layer vorticity in front of the tab around the tab. The second pair of vortices (UN and UP) are the vortices that are most probably shed from the sides of the tab. Finally, the third pair of vortices (PN and PP), which is the most dominant pair, are the vortices that are generated due to the surface pressure gradient setup in front of the tab.[90,91] These are the first direct measurements of these vortices in such a complex flowfield and an attest to the capabilities of the PDV technique. Details of these measurements can be found in Refs. 69 and 88.

State of the PDV Technique

The PDV technique is only several years old, but from what has been discussed so far, it is apparent that the technique has been developed into a capable velocimetry technique and that it holds

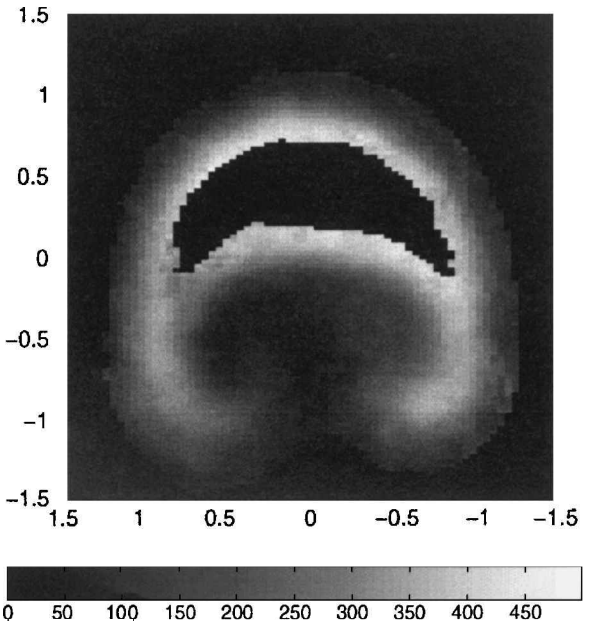

a) Mean streamwise velocity (x component) map

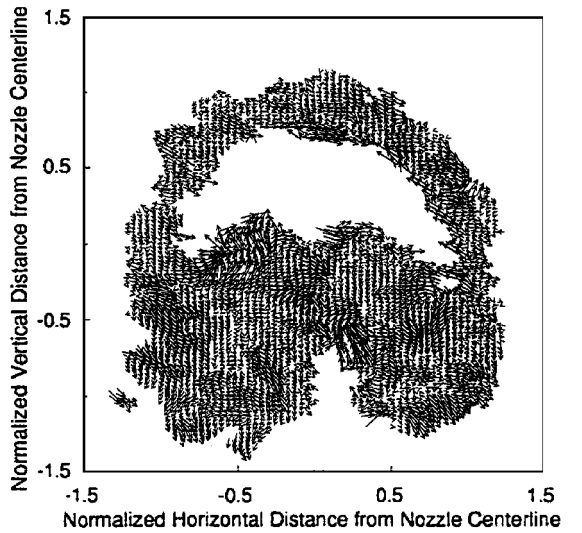

b) Instantaneous cross-stream velocity vectors (y–z plane)

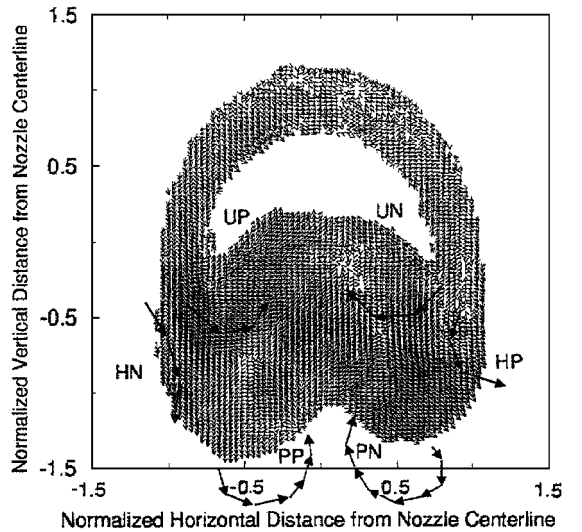

c) Mean cross-stream velocity vectors (y–z plane)

Fig. 14 Mach 2 tabbed jet.

great promise to provide detailed and accurate measurements, especially in high-speed flows where such measurements are desperately needed. Currently, only several groups in the United States and around the globe are actively pursuing the development of this technique. Even with limited time and activity levels, PDV has been developed into a powerful technique that can provide relatively accurate three-component velocity results in high-speed flows. With this kind of success, more researchers will adopt the technique and will work on the areas of concern to make the technique more accurate, robust, user friendly, and economical. Rather than presenting uncertainties and errors associated with the PDV technique, several areas that are in need of further understanding and improvement will be discussed. Detailed uncertainty analyses can be found in the earlier cited references.[9–33,87]

As was discussed earlier, there are several areas in the PDV technique that are in need of further improvement and advancement, only three of which need major improvement for the technique to strive and to become widely used in the laboratories. These areas are 1) laser power fluctuations and drift, 2) image registration and its associated issues, and 3) the speckle noise. Each one of these will briefly be discussed.

Laser Power Fluctuations

The laser power fluctuations and drift were discussed earlier. A simple system that consists of two fast-response diodes and an additional iodine filter can easily be used to monitor the laser frequency variations and to incorporate them into the calculations.[14,16,18–22] As was seen in the results presented in Fig. 11, this is an effective way of dealing with the laser frequency variations. However, its incorporation into the PDV system makes the technique a little more complicated. This can be overcome more effectively by the laser manufacturers, if they see a market for the improved laser.

Image Registration

As was discussed earlier, the pixel-to-pixel image matching is at the heart of the PDV technique. It occurs in several stages in the PDV technique: 1) in obtaining filter profiles, 2) in obtaining flatfield images, 3) in matching the filtered and unfiltered images (Fig. 2) in the Doppler shift calculation stage, and 4) in matching the images among two or three cameras in the velocity calculation stage (Fig. 9). If this pixel-to-pixel matching is carried out properly, then the effects other than the instantaneous Doppler shift, such as particle size, particle number density, and the optical effects of the split image system, are removed. Smith et al.[15] and Clancy and Samimy[17] have shown that the matching must be within a subpixel accuracy for accurate measurements. As was shown in Fig. 13, the proper pixel-by-pixel matching of the images is crucial for obtaining accurate measurements.

Speckle Noise

When coherent light is scattered by scatterers of a nonuniform distribution, a detector will receive light of nonuniform phase that will interfere and form a pattern that is called a speckle pattern. Even though the scrambling of the phase of the coherent light is a random process, the speckle pattern is repeatable if the scattering medium is stationary and the locations of the laser and detector are fixed.[95] However, with a moving medium, the speckle pattern is a function of both time and space. This speckle noise is the main cause of the grainy nature of the instantaneous PDV images.[14,18,19,87] Because the speckle pattern is randomly distributed in time and space, it cancels out from the mean velocity and vorticity measurements. However, it is the major source of the uncertainties in the turbulence measurements.

In the PIV technique, one of the modes of operation is when the particle number density in the flow is high and a group of particles form a speckle pattern that moves in between two successive images. From the translation of the speckle pattern in between two images, the velocity of the particles traveling in a group is obtained.[37] When PIV is operated in this mode, it is called laser speckle velocimetry (LSV). When the optical path length difference of scattered light received by a detector, which is an indicative of the particle size and distribution, is larger than the wavelength of the illuminating light, then the speckle pattern is a function of the optics.[14,87,96–100] Obviously, this makes the LSV technique possible. It also gives clues on what are the parameters in an optical setup that one can modify to reduce the speckle noise in PDV. There are a couple of ways of deriving an equation for the speckle signal-to-noise ratio (SNR).[14,87,101,102] One way to derive speckle SNR[87,101] is

$$\mathrm{SNR} = \Delta x/(\lambda f\text{-number}) \tag{10}$$

where f-number is the ratio of the focal length to the aperture of the lens and Δx is the pixel size. From Eq. (10), it is obvious that one needs to reduce the f-number of the lens and also to increase the pixel size in the CCD camera to reduce the speckle noise. There are some variations in the pixel size in the CCD cameras, and one has to use a CCD camera with the largest possible pixel size. Smith[87] suggests using of inexpensive 8-bit CCD cameras with a larger pixel size than the more expensive scientific-grade 14- or 16-bit CCD cameras. One has to be cautious in doing so because these 8-bit cameras would provide lower speckle noise, but would also reduce the dynamic range by a factor of 64, in comparison with 14-bit cameras. McKenzie[13] has discussed in detail the main drawbacks of using an 8-bit camera in PDV. A large dynamic range of the imaging system is very important in using PDV in high-speed, highly turbulent flows.

Smith[87] experimentally validated Eq. (10) in terms of the effects of reduction of f-number on the reduction of speckle noise. However, there is a limit in lowering the f-number in the PDV technique to reduce the speckle noise. In a very small f-number lens, there would be variations in the Doppler shift on the image plane due to the variations in the observation angle (variations in $\boldsymbol{s}$ in Fig. 2). In fact, this variation of the scattering angle in a small f-number lens is the basis for the filtered angularly resolved Rayleigh scattering technique that has been used for simultaneous, single-point, density, temperature, and velocity measurements.[66,67]

In the image processing stage of the PDV results, one can also reduce the speckle noise. This requires using some sort of spatial image filtering. Clancy[69] and Clancy et al.[18,19] explored several different filters and discussed the most effective way of reducing the speckle noise. In the spatial resolution discussion, it was shown that the optical diffraction limits the spatial resolution of PDV. In the given example, the spatial resolution of PDV was determined to be approximately 75 μm. Therefore, using scientific-grade CCD cameras with much larger pixels, if available, or using standard scientific-grade CCD cameras but binning a few adjacent pixels in the data processing stage would not deteriorate the resolution of PDV. It would rather reduce the speckle noise and also would reduce the sampling error.[14] More work is warranted to clarify some of the issues discussed here.

As reflected in the title of the paper, the emphasis in this review has been on the application of PDV in high-speed flows. However, McKenzie[14] has shown that one can resolve flow speeds as low as about 2 m/s with PDV. Therefore, PDV seems to be also suitable to low speed, but large wind-tunnel applications, and may be able to compete favorably with PIV in such cases because PIV cannot resolve individual particles at large distances. Beutner et al.[30,31] have recently carried out some work in the application of PDV in large low-speed facilities.

PIV

PIV is a technique for measuring the in-plane two-component velocity field of a flow seeded with small particles. A pulsed laser light sheet is used to illuminate the particles entrained in the flow. The light scattered by the particles is collected normal to the plane of the light sheet and is imaged onto a photographic plate or a CCD camera, where the positions of the particles are recorded at each instant the light sheet is pulsed (Fig. 15). In high-speed flows, high pulse energy lasers are required to provide sufficient light energy ($\sim$100 mJ/pulse) in a short time interval ($<$10 ns) to record an unblurred image of the particles entrained in the flow. The data processing consists of either dividing the image up into small interrogation regions and determining the average displacement of the particles or by determining the individual particle displacements between pulses of the light sheet. Knowledge of the time interval between light sheet pulses then permits computation of the flow velocity:

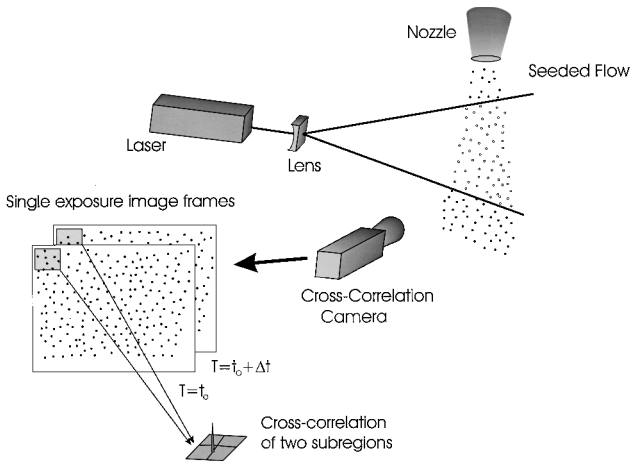

Fig. 15 Schematic layout of a standard PIV setup.

$$V = \Delta x/(M \cdot \Delta t) \tag{11}$$

where Δx is the measured displacement, M is the optical system magnification, and Δt is the time between exposures. The average displacement estimation technique yields a regular velocity vector grid, easily compared to computational fluid dynamics (CFD) predictions. The individual particle displacement estimate technique produces a random vector field. The number of exposures per frame and the seed particle concentration determines which data processing schemes are employed.[103] Whereas each technique has some inherent benefits, the appropriate choice depends on the characteristics of the flow and recorded image constraints. The PIV technique is also capable of providing three-component velocity measurements over a plane. As will be discussed, the addition of a second camera in a stereo viewing arrangement yields all three velocity components.

Overview of PIV

The discussion presented here concentrates on the PIV technique and its implementation for high-speed flows. The types of data processing used, the optical recording system constraints, and the illumination systems required for high-speed flows will be presented. For a more comprehensive overview of the PIV technique and the myriad of implementations covering low-speed to high-speed flow the readers are referred to Adrian,[37] Grant,[38] or Raffel et al.[104]

Light Sources

PIV relies on the use of high-accuracy pulsed laser illumination systems to record the particle positions at multiple instances in time. The Nd:YAG laser has several desirable qualities for use in PIV: near Gaussian beam profile, high timing accuracy (< 2-ns jitter), short pulse duration (< 10 ns), high per pulse energies (100 mJ/pulse), and a second harmonic wavelength in the green that closely matches the peak spectral responsivities of CCD cameras and film. Several commercial vendors offer dual-head Nd:YAG laser systems specifically for use in PIV applications. These dual-head systems use beam combining optics and a common frequency doubling crystal to simplify alignment and maintain collinearity of the laser beams. The dual-head feature also means that there are no restrictions on the minimum time between laser pulses; hence, high-speed to low-speed flows can be investigated using these types of laser illumination systems.

Sheet Forming Optics

The near Gaussian intensity beam from Nd:YAG lasers is easily formed into a light sheet through the use of spherical and cylindrical optics. Nominal light sheet thicknesses are on the order of 1 mm. The width of the sheet depends on the area of the flow under study and can also be restricted by the available pulse energy. Restrictions on the available optical access and experiment/facility geometry may preclude using conventional optics to deliver the light sheet to the measurement location. For example, Wernet[105] used a small periscope probe for generation and delivery of a light sheet inside of turbomachinery.

Data Processing

In theory, the type of data processing used to reduce PIV data is independent of the flow velocity. In reality, this is not always the case because the seed particle dynamics, the time between laser light sheet pulses, the duration of the pulses, and the framing speed of the recording system all place practical restrictions on the maximum velocity that can be recorded and processed using PIV. Each of these limitations will be discussed as they relate to obtaining high-speed velocity data. Basically, there are three types of data reduction techniques used in PIV: autocorrelation, cross-correlation, and particle tracking. The choice of a processing technique depends primarily on the available equipment used to record the particle image data and the seed particle concentration.

Correlation-based processing techniques produce spatially averaged velocity estimates. The recorded image frame is divided into small subregions, each containing particle images. By processing the image over a regular grid of small subregions, a velocity vector map is generated. The optimum number of particles per interrogation region for PIV is nominally 10 particle image pairs.[106]

Autocorrelation processing is the oldest of the PIV processing techniques, essentially because film-based recording systems were incapable of recording independent particle image records at two closely spaced instances in time. Single-exposure electronic image acquisition systems suffered from the same limitations as film plates and thus also relied on autocorrelation processing. In the autocorrelation technique a single image frame is exposed multiple times ($\geq$2) and processed over a regular grid of small subregions. For a double-exposure case, the average displacement of the recorded particle image pairs is determined by computing the autocorrelation of each subregion.

The two-dimensional autocorrelation is a symmetric function having a characteristic central peak at the origin of the correlation plane and two satellite peaks, oriented symmetrically about the central peak. The central peak originates from the correlation of all of the particle images in the subregion; hence, the size of the central peak is related to both the total number and size of the particles in the subregion. For more detailed discussion of the autocorrelation technique refer to Adrian.[106] The satellite peaks originate from the average displacement of the particle image pairs between exposures. For the displacement peaks to be discernable from the central peak, the particle displacements must be greater than the average particle diameters across the subregion. This requirement places a dynamic range limitation on the autocorrelation technique. A second shortcoming is in the symmetry of the autocorrelation function. The existence of two diametrically opposed displacement peaks about the central peak yields a 180-deg directional ambiguity in the velocity vector direction. The directional ambiguity can be eliminated by imposing a central offset on the particle image records, whereby the particle images are mechanically shifted between laser pulse firings.[107] Image shifting introduces extra complexity in the experimental setup and also additional errors due to optical path differences resulting from the image shift. Kompenhans and Raffel[108] used a photographic film plate and image shifting to record the transonic flow over a pitching airfoil. The data were processed via autocorrelation and the recirculating flow above the pitching airfoil could not have been resolved without image shifting. Raffel and Kost[109] used photographic plates to record the coolant ejection flow at the trailing edge of a turbine blade. Autocorrelation processing of the image shifted data was used to reduce the supersonic flowfield surrounding the turbine blade and the trailing vortex caused by the coolant ejection. Krothapalli et al.[110] used a high-resolution digital camera and image shifting to record an underexpanded jet flow. The imaged area of the nozzle flow (1.73 $\times$ 1.15 cm) was processed over a 50 $\times$ 60 grid of points using autocorrelation, and time-averaged velocity vector plots were generated.

The second spatially averaged PIV data reduction technique, cross-correlation processing, is superior to the autocorrelation technique. However, this technique places more difficult demands on the recording system. In cross-correlation PIV, two single-exposure image frames must be recorded. Film-plate-based recording systems are incapable of providing two single-exposure image frames at an acceptable frame rate. Even electronic camera systems are

hard pressed to provide sufficiently high framing rates to enable cross-correlation data reduction. The cross-correlation operation is similar to autocorrelation where again the image frames are divided into small subregions. However, now a subregion from image 1 (recorded at the first laser pulse) is cross correlated with a subregion from image 2 (recorded at the second laser pulse). The resulting output on the correlation plane is a single peaked function, where the peak represents the average displacement of the particles across the subregion between the two laser pulses. The direction of the displacement is determined unambiguously because the images from exposures 1 and 2 are recorded separately. Because there is no self-correlation peak, even zero particle displacements can be measured; hence, the cross-correlation technique provides a higher dynamic range measuring capability than the autocorrelation technique.[103, 105, 111]

In contrast to the spatially averaged correlation techniques just discussed, particle tracking techniques attempt to identify the displacement of individual particles.[112] Both single- and double-exposure imagery have been used in particle tracking algorithms. Bryanston-Cross et al.[113] used double-exposure film to perform particle tracking on the flow in a transonic turbine cascade. Chana et al.[114] used an electronic camera to record double-exposure imagery of the flow in the rotator–stator region of a transonic turbine facility. Single-exposure data are again preferred because knowledge of the particle time history adds direction information that aids in the tracking process. Wernet[103] used single-exposure image data to track particles in a supersonic nozzle flow. Most particle tracking techniques require more than two single-exposure image frames to perform efficiently. The first step in particle tracking is to process the single-exposure images and determine the particle image centroid locations. The particle centroid information from all of the image frames in the sequence are then used to perform the tracking operation. The essential premise in particle tracking is that the distance and direction of all second-exposure particles in the vicinity of a first-exposure particle are used to project the location of a third-exposure particle. The distance and direction from a candidate second- to third-exposure particle is used to project the location of a fourth-exposure particle. A particle trajectory is validated when the projected particle locations are all correctly determined, from a candidate first-exposure in the sequence to the last.

For high-speed flows, obtaining more than two single-exposure image frames is difficult. Therefore, multi-frame (>2) tracking techniques are not readily applicable to high-speed flows. Correlation techniques succeed by extracting the average displacement of a group of particles in a subregion. For tracking techniques to succeed with only two single-exposure image frames, information from the surrounding displacements must be used in the tracking operation. There are two approaches for extracting the individual particle displacements based on the surrounding particle displacements: fuzzy logic and neural networks. Fuzzy logic techniques utilize a rule base (flow continuity) for allowed particle displacements.[115] Particle pairs close together must move in similar directions and must have similar magnitudes. Neural net approaches to data extraction rely on training the nets to identify patterns.[38, 116] The nets must be trained on similar flows that they will be used to process. Determining the number of layers and training sets required for neural nets is similar to mixing paint, not much guidance is available and sometimes you get the desired results.

Alternatively, combining correlation and particle tracking techniques was proposed by Keane et al.[117] to create a PIV data processing system that can cover a wide range of flow seeding conditions and offer the potential for super-resolution PIV measurements. Particle tracking by itself is typically not capable of successfully tracking particles at the high seed particle densities normally used for auto- or cross-correlation analysis. Conversely, correlation techniques must use large subregion sizes, with a concomitant reduction in spatial resolution, in order to perform adequately in the low seed particle density regimes where particle tracking techniques are normally applied. In the combined technique, correlation analysis is first used to obtain a benchmark velocity vector map that then serves as a guide for the particle tracking operation. Hence, high seed particle images can be processed with small correlation subregion sizes, and then the spatial resolution of the measurements can be improved by following with particle tracking. For moderate density seed particle images, the correlation subregion size is increased so that a good velocity vector map is obtained, and then this is followed by particle tracking to obtain high spatial resolution measurements. For low seed particle density cases, the standard particle tracking can be used alone. Wernet[103] was the first to demonstrate the combined correlation/particle tracking technique in a supersonic nozzle flow. A high seed density flow was processed to obtain over 2300 individual velocity vectors in a 300-mm^2 area at a spatial resolution of 45 μm/pixel.

Image Recording Hardware

The general trend in PIV has been a migration away from film-based techniques, which require wet processing and cumbersome archiving, to electronic image acquisition. Electronic image acquisition, or digital PIV (DPIV), has enabled PIV to become a more useful tool in industrial and research applications. All electronic processing enables fast data processing and display so that the experimenter can determine the optimum experimental parameters while the experiment is being conducted. Another motivation for going to electronic image acquisition is the potential for obtaining a pair of single-exposure image frames, which would enable cross-correlation data analysis to be used. However, whenever high spatial resolution velocity measurements are required over a large field of view, film-based PIV is the technique of choice.

As stated earlier, film-based techniques are suitable for high-speed flows, but nearly always require auto-correlation data analysis. The exception to this rule is the two-color PIV work done by Post et al.,[118] where green and red laser sheets were used for flow illumination and color film used to record the particle image data of the flow in a turbine cascade. The color film was electronically scanned to create separate green and red image frames. The work pioneered by Post et al. has been continued by Estevadeordal et al.,[119] where the color film has now been replaced by a high-resolution color CCD camera. The two-color technique enables a single camera to be used to record high-speed flows and has been used to investigate the flow around an automotive cooling fan. However, there are a few restrictions: The particle images cannot completely overlap from the first to second exposure, the number of red and green pixels in the CCD sensor is not equal (1:2), chromatic aberrations keep the red and green particle images from being formed equally on the CCD sensor, and the energy available in the red light sheet is typically a fraction of the energy in the green light sheet.

Another approach for obtaining a pair of single-exposure image frames is to use a two-camera recording system. Wernet[103] demonstrated a two-camera recording system in a supersonic nozzle flow using high-resolution CCD cameras and polarization separation. A polarization beam splitting cube was used to obtain coaxial viewing of the illumination plane. The pulsed beams from two separate Nd:YAG lasers were combined, after frequency doubling, yielding two orthogonally polarized sheets, which enabled each camera to record light from only one of the illumination pulses. The submicrometer-sized seed particles used in this study did not significantly depolarize the scattered light. Image registration of the two-camera images was obtained using a calibration grid and image-warping algorithms.

Although a two-camera recording technique enables a pair of single-exposure image frames to be recorded, work still continued to reduce the complexity and cost of PIV optical recording systems. Of course, standard RS-170 [or phase alternate line (PAL)] video systems could be used to record single exposure image frames, but the video framing rate of 30 frames/s limited this approach to very low-speed flows. Wernet[112] was the first to demonstrate the frame straddling technique now used as the standard in the cross-correlation cameras found in commercial PIV systems. Wernet used the frame straddling technique in conjunction with particle tracking to measure a 150-m/s nozzle flow. In the frame straddling technique, the light from a pulsed laser source is made to coincide, or straddle, the vertical drive interval of a standard RS-170 video camera (or high-resolution 30 frame/s video system). In this way a video image frame is exposed just at the end of its integration period, and next video frame is exposed right at the beginning of its integration period. Hence, a pair of single-exposure image frames are obtained.

The standard 30 frame/s camera achieves a high effective framing rate capability via this technique. The time between image frames can be driven down to the vertical drive interval of the camera, which is on the order of a microsecond.

The adaptation of the frame straddling technology into commercial PIV systems has enabled the development of fast PIV data acquisition and reduction systems employing the optimal cross-correlation data reduction technique. These robust and extremely powerful commercial PIV systems have brought PIV out of the research laboratory into large-scale facilities. These commercial PIV systems provide fast processed velocity vector maps. The fast feedback enables optimization of the image processing parameters and a preview of velocity measurements being acquired. Commercial PIV systems based on this technology have been used to measure the intrablade flowfields in a 50-cm-diam transonic axial compressor operating at 17,000 rpm (Ref. 120). PIV has also been used to measure the flowfield in the diffuser of a high-speed centrifugal compressor operating at a pressure ratio of 4:1 and a design speed of 21,750 rpm (Ref. 111). Using PIV in rotating machinery applications has many advantages over previous measurements made using LDV. Both instantaneous and time-averaged velocity measurements can be made, which enables the investigation of nonstationary flow phenomena. The planar measurement capability of PIV significantly reduces the facility run time by over an order of magnitude over previous single-point measurement techniques such as LDV. Finally, by introducing the light sheet parallel with the diffuser and/or rotor hub, measurements can be obtained closer to the surface than previously possible using normal incidence LDV systems.

Raffel et al.[104] have also used cross-correlation cameras to study the flowfield behind an advanced aircraft propeller (velocity on the order of 80 m/s). Both instantaneous and time-averaged velocity vector maps on a 61×62 grid were generated from the 20×20 cm field of view images. Kooi et al.[121] used cross-correlation cameras to study the trailing wake flow behind an airplane half-plane model. The wind-tunnel freestream velocity was 60 m/s, and the area imaged by the PIV system was 0.2×0.2 m, with a spatial resolution of 0.2 cm/pixel. To visualize the wing tip vortices, the light sheet was oriented perpendicular to the primary flow direction. The resulting velocity vector maps contained a 60×60 grid of measurement points.

Seeding

A more general discussion of seed particle requirements has already been given in the Overview of PDV section and will not be repeated here. The type and size of seed material used is dictated by the specifics of the flowfield under study. In general, the seeding requirements for PIV are an order of magnitude higher than that required for LDV measurements.

Spatial Resolution

The spatial resolution obtainable using PIV is determined by the appropriate choice of seed particle density, camera field of view, and imaged particle size on the CCD sensor. Westerweel[122] presents a thorough discussion of these parameters and gives a general guide for the optimal PIV system configuration. Several factors must be optimized to obtain high spatial resolution measurements and yet avoid some of the systematic errors inherent in DPIV. Some of these factors have to be addressed before the data are acquired, and some are addressed in the data processing. The minimum error in estimating the displacement correlation peak is obtained when the imaged particle size on the CCD sensor is on the order of 1–2 pixels.[123] However, if the particle images are all on the order of 1–2 pixels and a centroid estimator is used to compute the displacement peak location, then peak locking can occur.[122] This phenomenon is observed quite frequently in airflows where the field of view is large and the imaged particle size is small. Proper selection of the recording camera lens f-number can be used to ensure that diffracted particle images are recorded that have the optimum particle diameter to pixel width ratio. A second factor to consider at the image recording stage is to ensure sufficiently high seed particle concentration. The ultimate spatial resolution of the processed velocity vector maps will depend on the seed particle concentration, as will be discussed further.

In the data processing stage, there is a tradeoff between resolution and accuracy in PIV measurements; however, we can attempt to maximize both by judicious design of the experiment. Following the discussion by Westerweel,[122] the reliability of the PIV estimate from a processed subregion improves as the number of particle image pairs increases. The correlation peak SNR is proportional to the total number of particle image pairs in the subregion, but the accuracy of the peak position estimate is not increased.

The error in the PIV estimates stems from the timing of the laser light sheet pulses and the estimate of the particle displacement. The laser timing is very accurate and does not significantly contribute to the error in the velocity estimates. The accuracy of PIV displacement estimates is primarily determined by the ratio of the correlation peak size d_r to the subregion size N:

$$\sigma_{\Delta x} = d_r / N \tag{12}$$

The maximum displacement on the correlation plane is limited by the subregion size. To avoid aliasing in the correlation plane, the displacement search region must be restricted to one-quarter of the subregion size.[106] By using three-point Gaussian interpolation techniques, the correlation peak position can be estimated to subpixel accuracy.[122] Nominal values for the peak position error are on the order of 0.1 pixel for particle images spanning 1–2 pixels on the subregion. Combining the one-quarter rule with the peak position accuracy sets the full scale accuracy of the PIV velocity estimates. Assuming a PIV subregion size of 64^2 pixels, and applying the one-quarter rule described earlier, the relative error in the displacement is approximately $0.1/16 \approx 0.6\%$. For a 1024×1024 pixel image, processed with 50% overlapped subregions, a 32×32 grid of vectors would be obtained. In this case we have optimized the measurement accuracy while sacrificing spatial resolution.

The lower limit on the spatial resolution of the velocity measurements is set by the actual particle displacement between the illumination pulses. Large displacements between exposures are desirable to achieve high-accuracy velocity estimates. In standard correlation processing, subregions that are larger than the spatial scale of the particle displacement are used in order not to violate the one-quarter rule. By incorporating subregion shifting in the data processing procedure,[122] reasonable precision velocity estimates can still be obtained while simultaneously increasing the spatial resolution of the measurements. In cross-correlation processing, the second correlation subregion can be spatially shifted with respect to the first subregion by an amount equal to the mean flow displacement between exposures, which keeps the correlation peak at the center of the correlation plane and minimizes any distortion effects caused by the windowing of the fast-Fourier-transform-based correlation operation. Employing subregion shifting also enables the use of smaller interrogation regions, provided the smaller subregions still contain a sufficient number of particles to provide a correlation result. Therefore, subregion shifting enables the measurement of displacements larger than prescribed by the one-quarter rule. If we now use a 32^2 pixel subregion to process the same 1024×1024 pixel image using 50% overlapped subregions and an 8 pixel subregion shift, then the accuracy of the velocity estimate is still the same as before, $0.1/16 = 0.6\%$, and the processed velocity vector map now contains 64×64 grid points. The velocity precision has been maintained, and we have increased the spatial resolution by a factor of two in each dimension. The spatial resolution now matches the lower limit spatial resolution set by the particle displacement (assuming the particle displacements were on the order of 16 pixels for the two cases just described and 16 pixel spacing between subregions centers). The general trend is summarized in Table 1, again assuming that subregion shifting is employed. Throughout the discussion of the various implementations of PIV data processing and image acquisition hardware above, the specific resolutions for some of the references have been listed for comparison.

Dynamic Range

The PIV technique has been used extensively to measure low-speed flows; however, our focus in this work is on high-speed flows. From Eq. (11) we see the parameters that affect the range of velocities that can be measured using PIV. Because the time between laser pulses can be arbitrarily large, very low velocities are easily

Table 1 PIV spatial resolution vs precision

Subregion size	Velocity accuracy, % of full scale	Number of grid points in processed vector map
16 × 16	2.5	128 × 128
32 × 32	1.25	64 × 64
64 × 64	0.6	32 × 32
128 × 128	0.3	16 × 16

measured. As we attempt to measure higher speed flows, we must reduce the time between laser pulses to record the particle positions before they travel out of the field of view. In cross-correlation PIV, the minimum Δt that can be used is not limited by the laser, but instead is limited by the camera used to record the pair of single-exposure image frames. The minimum Δt for the currently available cross-correlation cameras is on the order of 1 μs. Measurements of transonic flows are possible using this time delay on a 50 × 50 mm field of view.[105] When the time between image exposures can no longer be shortened, another option is to decrease optical system magnification M in Eq. (11), which increases the field of view. The magnification cannot be increased past the point where we can no longer resolve the images of the individual particles. If the particle images become too small and only span a single pixel, then peak locking will occur.

In addition to the parameters that are manipulated at the time of image acquisition, there is another option that can be exercised in the data processing stage that will extend the operating range of PIV measurements. The size of the correlation subregion limits the maximum velocity that can be detected as stipulated by the one-quarter rule (average displacement cannot be larger than one-quarter of the subregion size). When the average particle displacement between exposures becomes larger than can be accommodated within the desired subregion size, then subregion image shifting can be employed. Subregion image shifting adds a dc offset to the second correlation subregion in the mean flow direction. Hence, if we can no longer keep the distance the particles move between exposures short, we can offset the processing regions to augment the limitations of the recording hardware. Subregion image shifting is readily applied in high-speed flows where the convective flow is much higher than any spatial structures in the flow. The main assumption made here is that the flow is predominantly two-dimensional because significant out-of-plane motion would preclude capturing the particles in exposure 1 at a later time in exposure 2.

The preceding section discussed the spatial resolution considerations in PIV. Here we have shown that some of the parameters affecting spatial resolution are also important in determining the maximum velocity that can be measured using PIV. Although the PIV technique has seen a majority of application in low-speed flows, by proper optimization of the image recording and correlation processing steps, high-speed flows can easily be measured using PIV.

Three-Component PIV

Although PIV has made two-component planar measurements in low-speed flows rather commonplace, many flows of interest are fully three-dimensional and, therefore, do not posses a plane of symmetry for easy two-component, planar measurements. In addition, two-component measurements leave out half of the Reynolds stresses required to understand the physics of turbulent flows. Many approaches have been investigated and proposed for obtaining three-component velocity information utilizing the PIV technique. These approaches can be broken into three separate classes: three-component velocity measurements in a volume; two-component measurements across multiple planes, and three-component velocity measurements across a plane. Most of the volumetric approaches are limited to tracking a relatively low number of particles in the volume in very low-speed flows and suffer from particle overlap ambiguities.[124] Holographic techniques have also been proposed and demonstrated for volumetric three-component velocity estimates via particle tracking.[125] Another approach for obtaining volumetric three-component measurements is by rapidly scanning a laser sheet or by using a color coded laser sheet.[126,127] All of the mentioned techniques have only been applied in low-speed flow applications.

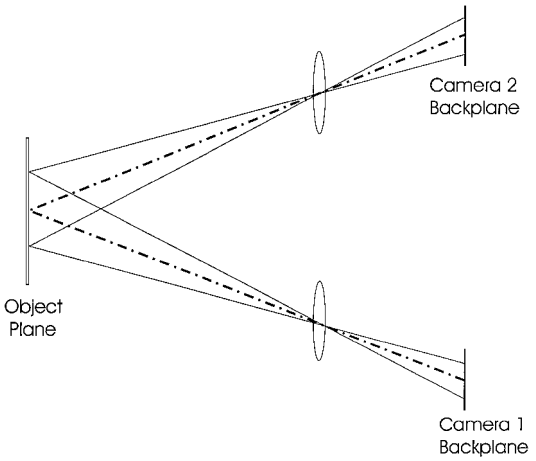

a) Lens translation configuration

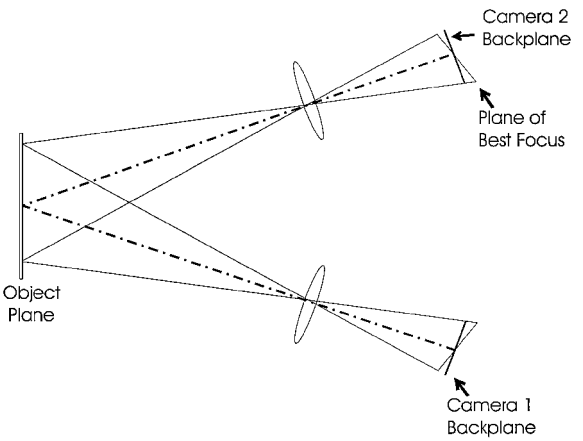

b) Angular displacement configuration

Fig. 16 PIV configurations.

The planar measurement region techniques are simply an extension of the in-plane two-component PIV technique. In the planar approach, multiple recording cameras are used in a stereo viewing configuration.[128] There are two primary configurations for stereo PIV: lens translation and angular displacement, as shown in Figs. 16a and 16b. Lens translation is simple and for small field angles results in no appreciable optical distortion.[92,128,129] The common image area from the two cameras may be restrictively small unless the field angles are enlarged. Using large field angles in the displacement technique increases the sensitivity to the out-of-plane displacement, but will also produce perspective distortion in the image.[130] The angular displacement technique is considered to be more accurate; however, this technique results in perspective distortion on the image plane and typically requires a large depth of field to avoid defocusing across the image plane.[125,128] The image plane of best focus does not fall on the straight back camera film plane, resulting in blurring at the edges of the image. The use of high f-number collection optics increases the depth of field and minimizes the blurring. The errors of perspective distortion can be ignored by keeping the coupling angle between the cameras small; however, sensitivity to the out of plane component is reduced.[93,113,131] The large depth of field requirement of the angular displacement technique is easily eliminated by tilting the film plane such that the Scheimpflug condition is satisfied.[123,132] The Scheimpflug condition requires that the image plane, object plane, and the median plane through the lens all intersect at a common point (Fig. 17). The tilted object plane is imaged onto a tilted image plane where all points are in focus and the depth of field requirements of the optical system are reduced. The object to image distances vary horizontally across the image, resulting in perspective distortion. Both the vertical and horizontal magnification varies as a function of horizontal position on the image plane. These distortions can be accounted for in the data processing using image warping or an

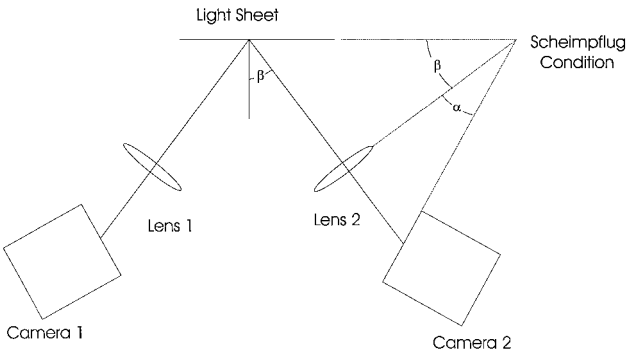

Fig. 17 Schiempflug configuration of a stereo viewing optical setup for PIV.

exact analytical transformation.[132] The advantages of the angular displacement technique are the large field of view and the improved accuracy in estimating the out-of-plane displacement. An indirect advantage of the stereo view configuration is the collection of the particulate scattered light from an angle other than 90 deg from the scattering plane. The scattering efficiency reaches a minimum at 90-deg collection for polarized light; therefore, the oblique collection angles collect more light than would be detected from a standard PIV setup. In some standard two-dimensional PIV applications, 90-deg viewing is not feasible, and the Scheimpflug off-axis viewing provides an alternative.[132]

The errors associated with the angular displacement technique are similar to those for a three-component LDV system. The error in the z component of velocity is dependent on the two in-plane x-component velocity estimates. For PIV the in-plane velocity estimates can be 1% of full scale for an optimized experimental setup. For a stereo viewing optical system, the error in the out-of-plane displacement component is $\sigma_{\Delta x}$ to first order given by Wernet,[51]

$$\sigma_{\Delta z} = \sigma_{\Delta x} / \tan \beta \tag{13}$$

where $\sigma_{\Delta x}$ is the in-plane error in the x component of displacement and β is the coupling half-angle between the two optical systems. Hence, we obtain the result that the error in the out-of-plane displacement is inversely related to the tangent of the optical system coupling half-angle. This simplification allows us to define an approximate ratio of the error in Δz to the error in Δx. For the case where $\beta = 30$ deg, the error in Δz is 1.7 times as large as the in-plane error Δx. At the limit of $\beta = 45$ deg, the error in the out-of-plane displacement equals the in-plane displacement error.

Except for that of Funes-Gallanzi and Bryanston-Cross,[131] all of the three-component measurement systems described were used in low-speed flows. They used a stereoscopic PIV system to measure the flow around an airplane model with velocity up to 60 m/s. Wernet[51] used a Scheimpflug configuration stereo viewing PIV system to obtain three-component velocity slices in a supersonic nozzle flow at several axial positions in the flow. In this work, the light sheet was oriented perpendicular to the main flow direction, which is not the optimal configuration for obtaining high-accuracy measurements, but is significant in that the measurements were obtained at all. In a similar optical configuration (light sheet perpendicular to the main flow direction), Raffel et al.[104] used a long-range (9-m) stereo PIV system to make three-component velocity measurements in a study of blade tip vortices from a rotorcraft model. The maximum velocities measured were on the order of 50 m/s and the observation area was 25 × 30 cm, yielding a processed velocity vector map containing a grid of 51 × 61 vectors.

Sample PIV Results

A PIV flowfield study was conducted on a 50.8-cm-diam, single-stage axial compressor with a design speed of 17,188 rpm and a mass flow rate of 20.19 kg/s, yielding a pressure ratio of 1.86 (Fig. 18). The rotor has 36 blades with a span of 75 mm at the leading edge and 56 mm at the trailing edge. The blade stagger angle is 41 deg at the hub and 61 deg at the tip. The casing is fitted with a large optical access window (200 × 100 mm) that is molded to the complex contour of the casing. The glass thickness is 3 mm and produces a very small amount of optical distortion. None of the optical distortion effects will be considered here.

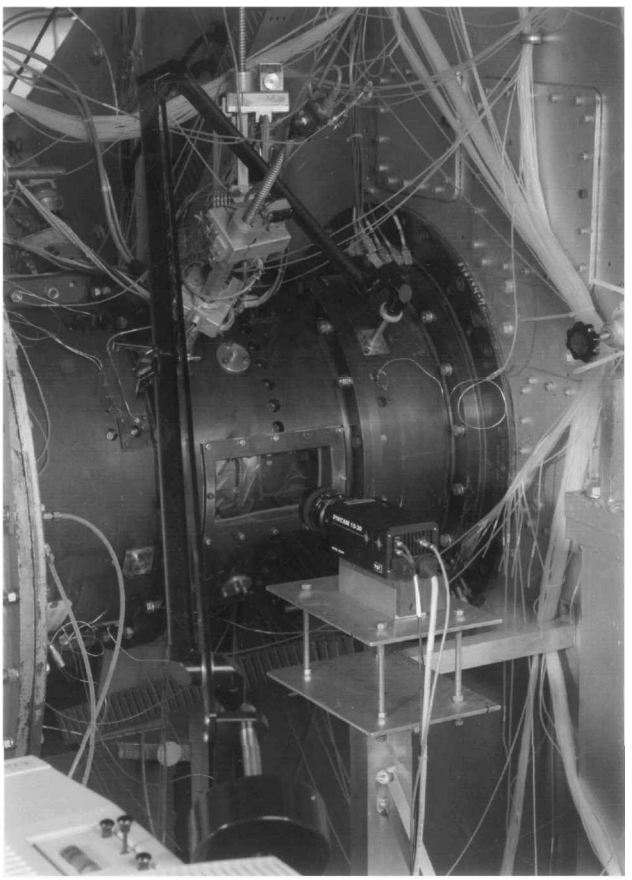

Fig. 18 PIV installation in an axial compressor facility.

A very compact light sheet delivery system was constructed using a periscope-type configuration. The pulsed Nd:YAG beam is directed down the bore of the tube that contains light sheet forming optics and a 90-deg turning mirror. A 1000 × 1000 pixel cross-correlation CCD camera with 9-μm square pixels was used to image the flow. Although the spatial resolution of the optical system is much larger than the actual geometric image of the particle on the CCD sensor, the diffraction effects of the optical system may produce effective particle images that are much larger.[106] For example, a PIV image recording system using a f-number 5.6 camera lens operating at a magnification of 0.16 and using an illumination wavelength of 532 nm yields a 9-μm-diam point spread function on the CCD sensor. The optical system point spread function is matched to the CCD sensor resolution. The submicrometer-sized seed particles used in this study ended up being imaged to objects on the order of the CCD pixel size and, hence, resulted in a minimal correlation peak centroid estimation error.[122]

The seeding was provided by a 6 jet atomizer (producing 0.7-μm-diam particles using Rosco's smoke juice) that injected seed through a 6-mm-diam seeding probe located approximately 80 probe diameters upstream of the rotor. The seeding probe position could be adjusted radially to provide seed in the plane of illumination. The light sheet was introduced into the rig via the optical periscope probe. A commercial articulated light arm was used to couple the light from a dual-cavity Nd:YAG laser system to the periscope probe. The light sheet pulse energy was approximately 125 mJ/pulse. The probe was inserted through the casing at a circumferential position 45 deg below the rig centerline and approximately 200 mm upstream of the rotor. The inclination angle of the light sheet roughly matched the blade stagger angle at both midspans. The light sheet generated by the probe was approximately 45 mm wide and 1 mm thick at the measurement location.

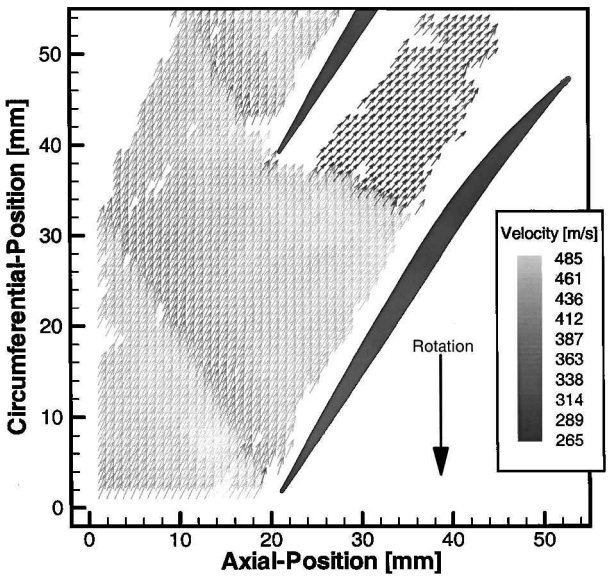

Fig. 19 Instantaneous velocity vector map of the flow in the transonic axial compressor.

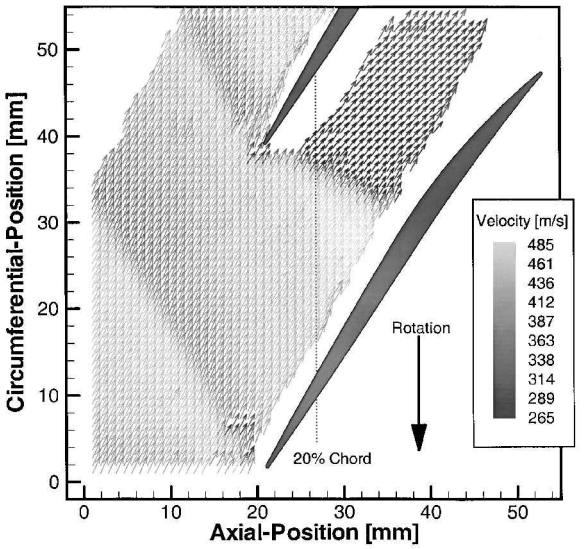

Fig. 20 Velocity vector map, 96 frame average, of transonic axial compressor flow.

The camera image scale factor was 56 μm/pixel, yielding a 56 × 56 mm field of view, and the interframe time was 2.67 μs. The lightsheet illumination covered most of a blade passage in the circumferential direction at a passage height of 46 mm from the hub (70% span). The plane of the lightsheet intersected the lower blade at constant radius, but was slightly inclined along the pressure surface of the upper blade. The flow velocity upstream of the rotor is 190 m/s, and the blade speed at the measurement plane is 390 m/s. The flow direction is from left to right, and the rotational direction is from top to bottom. The blade profiles at the measurement plane location are shown in Figs. 19 and 20. The vectors in Figs. 19 and 20 are shown in the relative frame (wheel speed has been added) and are scaled in proportion to velocity vector magnitude and also gray scale coded by vector magnitude. The data were processed using a cross-correlation subregion size of 32 × 32 pixels (1.8 × 1.8 mm subregions) with 50% overlap. A subregion shift of (8, −4) pixels in the x and y directions was used so that smaller sized subregions could be utilized. Spurious vectors located around the blade surfaces and in the periphery of the image have been removed. No interpolation or data filling has been applied. Figure 19 shows an instantaneous vector map of the flowfield. Figure 20 shows a 96 frame average velocity vector map. Under these rig operating conditions, a strong shock forms off the upper blade leading

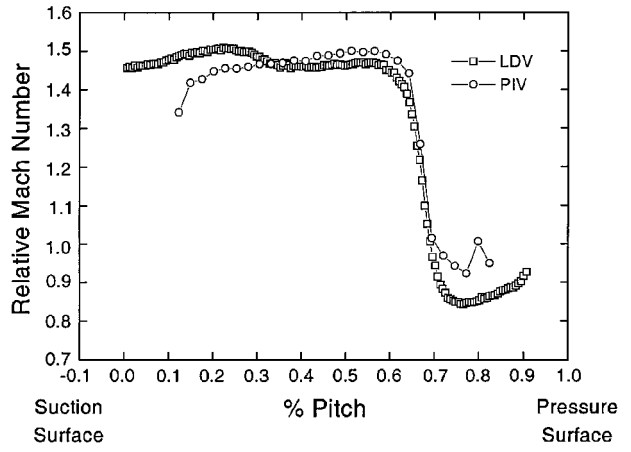

a) Relative Mach number vs percent pitch for PIV and LDV

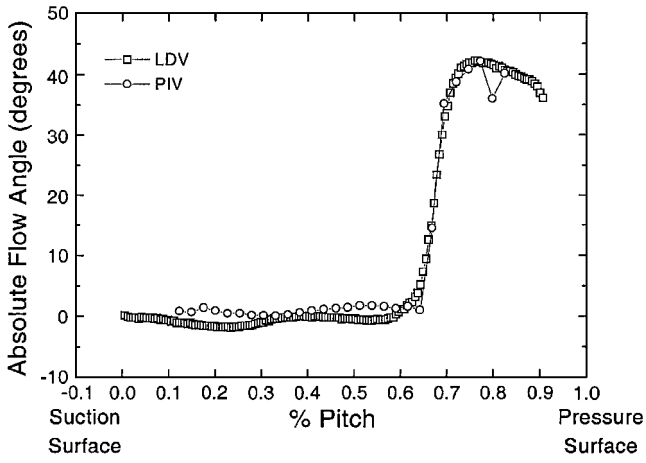

b) Flow angle vs percent pitch for PIV and LDV

Fig. 21 Comparison of PIV and LDV measurements at 20% chord for the velocity vector map shown in Fig. 20.

edge and spans the blade passage. The position of the blade-to-blade plane shock is readily observed by the sharp drop in vector magnitude within the blade passage (light to dark shading). A bow wave also forms off of each blade extending outward (up and to the left) from each blade leading edge. The bow wave from both the lower and upper blades are observed in the left portion of the image. There is also a significant change in velocity magnitude across the bow waves as indicated by the gray shading (medium gray vectors). The average velocity vector map in Fig. 20 is smoother and has more filled in areas than the instantaneous vector map shown in Fig. 19.

Previous LDV measurements acquired in the same facility under similar conditions will be used to assess the quality and accuracy of the time-averaged PIV data (A. J. Strazisar, 1997, personal communication). The vertical line inside the blade profiles in Fig. 20 indicates the 20% chord position along the blade at 70% span. Figure 21a shows the relative Mach number vs percent pitch measurements obtained using PIV and LDV, respectively. The LDV measurements were obtained at a higher sampling density across the blade pitch (200 points) and are closer to the blade surfaces than the PIV measurements (29 points). Both systems show the blade-to-blade shock occurring at approximately 65% pitch. Both sets of measurements show the shock spanning about 15% of pitch. Figure 21b shows the absolute flow angle vs percent pitch measurements obtained using PIV and LDV. Again the measurements between the two techniques are in very good agreement, spanning essentially the same range and exhibiting similar features.

Summary

As the title of this review indicates, the focus here is on planar, multiple-component, velocimetry in high-speed flows. High-speed flows are almost always of very high Reynolds number and

highly turbulent. Thus, these flows possess very large dynamic range in velocity, length, and timescales. An ultimate velocimetry technique that would help in exploring the physics of such flows would provide detailed, accurate, volumetric, real-time, instantaneous velocity data. From the discussion so far it is obvious that we are not anywhere near this goal, but making steady progress toward it. The volumetric and real-time aspects are harder to achieve in high-speed flows at this time. Currently, there are two planar velocimetry techniques that are developing rapidly into useful tools and could provide detail and accurate instantaneous velocity information in high-speed flows, if designed and utilized properly. The techniques are PDV and PIV. The details and state of the art of both techniques were presented and discussed. Which one of these techniques is preferred over the other depends on many factors, such as the objectives of the measurements, the level and the dynamic range of expected velocities, the spatial resolution requirement, the accessibility of the flowfield, and of course the availability of both the expertise and necessary equipment. Next, these issues will be briefly discussed.

From the discussion, it is apparent that two-component PIV in low to moderate speed flow applications is a well-developed technique with commercially available complete hardware and software packages. The setup and application of these commercial two-component PIV systems is relatively simple, and the fast feedback of velocity data enables online optimization of the image recording parameters. For low to moderate velocity two-component applications, PIV is a better choice at this time due to its simplicity and ease of implementation. As the velocity approaches supersonic speeds, PIV is limited due to the image capture capabilities of the cross-correlation cameras. Three-component PIV is just becoming commercially available and still requires quite a bit of expertise for accurate measurements.

The PDV technique is developing rapidly and holds great promise, especially in high-speed flows and in large facilities. However, neither the hardware nor the software for PDV is available off-the-shelf, and a successful design and application of the technique requires substantial in-house development and expertise. Therefore, not only the availability of the necessary equipment, but also the availability of in-house expertise, is a deciding factor in the selection of a technique. Optical access restrictions in some facilities could also adversely affect the accuracy in some of the resolved velocity components.

As for the objective of the research, if it is to obtain mean velocity and some components of Reynolds stresses in a 50×50 grid on a given plane so that a CFD code and its turbulence models could be examined and improved, then either PIV or PDV would be able to accomplish the task. However, if the objective is to obtain detailed, high-resolution turbulence data, so that one can understand the physics of the turbulence field, then PDV offers a better choice. As was discussed earlier, the speckle noise, which necessitates the binning of several adjacent pixels in image processing stage, could limit the spatial resolution of PDV. However, as was shown, in a high Reynolds number laboratory-scale supersonic jet, the spatial resolution of PDV is perhaps diffraction limited. Whether diffraction or speckle noise limited, PDV still offers a higher spatial resolution velocity measurement capability than PIV.

We have chosen to make generalized statements in comparing PDV and PIV systems, based on our understanding of and experience with the techniques, because no direct comparison measurements are available at this time. We would also acknowledge that PDV systems capabilities are improving whereas those of PIV are mature. To make a meaningful head-to-head comparison between these two techniques, the comparison must be done on an object space spatial resolution basis (defining the limiting velocity measurement grid spatial resolution in physical units). Comparisons based on the number of pixels used in a PIV correlation subregion or binning of several adjacent pixels in PDV are not precise due to the many parameters that combine together to determine the actual spatial resolution of the measurements such as the field of view of the recording system, the pixel count and size in the CCD sensors, and the oblique viewing angle of the illumination plane.

The flow velocity and dynamic range are very important considerations. As the flow velocity increases, the magnitude of the Doppler shift for a given setup increases. This would improve the accuracy of PDV. On the other hand, PIV has to balance the accuracy of measuring shorter transit time with the required spatial resolution. This problem is aggravated as the dynamic range is extended. However, it has been shown that with proper arrangement PIV can be used in high-speed flows. In small facilities, if accessibility to the flowfield is limited and if only two-component measurements are desired, then PIV would be a better choice. For example, one small window is needed to bring the laser sheet into the flow in both PIV and PDV, whereas PIV requires one additional window to collect the images and PDV requires two additional windows. If three-dimensional measurements are required, the stereo viewing PIV system can view the measurements volume through a single large window; however, the PDV system will require three windows to obtain three-component velocity measurements. If the three windows are available, then PDV would be preferred because it would provide a better spatial resolution. The PDV technique would be preferred in large facilities because the imaging of individual particles and, thus, obtaining correlations would be difficult using PIV.

Acknowledgments

The first author gratefully acknowledges the support of his work in this area over the years by NASA, the Air Force Office of Scientific Research (AFOSR), the Office of Naval Research, and the National Science Foundation and the current support of NASA John H. Glenn Research Center at Lewis Field (with Khairul Zaman) and the AFOSR (with Steven Walker, Thomas Beutner, and Mark Glauser). He would like to thank three of his former students, Gregory Elliott of Rutgers University, Pamela Clancy of TRW, and Stephen Arnette of Sverdrup Technology, who have made significant contributions to the development of PDV, and also an anonymous reviewer whose thorough review of the PDV section helped to improve the quality of the paper. The second author would like to thank David Williams and A. J. Strazisar for their help in the operation of the transonic compressor facility. He would also like to thank W. T. John for his assistance in the setup and installation of the PIV system.

References

[1]Gharib, M., "Perspective: The Experimentalist and the Problem of Turbulence in the Age of Supercomputers," *Journal of Fluids Engineering*, Vol. 118, June 1996, pp. 233–242.

[2]Seasholtz, R. G., and Greer, L. C., III, "Rayleigh Scattering Diagnostic for Measurement of Temperature and Velocity in Harsh Environments," AIAA Paper 98-0206, Jan. 1998.

[3]Adrian, R. J., "Laser Velocimetry," *Fluid Mechanics Measurements*, edited by R. J. Goldstein, Hemisphere, New York, 1983, pp. 155–244.

[4]McDaniel, J. C., Hiller, B., and Hanson, R. K., "Simultaneous Multiple-Point Velocity Measurement Using Laser-Introduced Iodine Fluorescence," *Optics Letters*, Vol. 8, Jan. 1993, pp. 51–53.

[5]Cummins, H. Z., Knable, N., and Yeh, Y., "Observation of Diffusion Broadening of Rayleigh Scattered Light," *Physical Review Letters*, Vol. 12, No. 6, 1964, pp. 150–153.

[6]Yeh, Y., and Cummins, H., "Localized Fluid Flow Measurements with a He–Ne Laser Spectrometer," *Applied Physics Letters*, Vol. 4, No. 99, 1964, pp. 176–178.

[7]Komine, H., Brosnan, S., Litton, A., and Stappaers, E., "Real-Time Doppler Global Velocimetry," AIAA Paper 91-0337, 1991.

[8]Meyers, J. F., and Komine, H., "Doppler Global Velocimetry: A New Way to Look at Velocity," *Laser Anemometry*, Vol. 1, 1991, pp. 289–296.

[9]Elliott, G. S., Samimy, M., and Arnette, S. A., "Molecular Filter Based Diagnostics in High-Speed Flows," AIAA Paper 93-0512, 1993.

[10]Elliott, G. S., Samimy, M., and Arnette, S. A., "A Molecular Filter Based Velocimetry Technique for High Speed Flows," *Experiments in Fluids*, Vol. 18, 1994, pp. 107–118.

[11]Arnette, S. A., Samimy, M., and Elliott, G. S., "Two-Component Filtered Planar Velocimetry in the Compressible Turbulent Boundary Layer," AIAA Paper 96-0305, 1996.

[12]Arnette, S. A., Samimy, M., and Elliott, G. S., "Two-Component Planar Doppler Velocimetry in the Compressible Turbulent Boundary Layer," *Experiments in Fluids*, Vol. 24, 1998, pp. 323–332.

[13]McKenzie, R. L., "Measurements Capabilities of Planar Doppler Velocimetry Using Pulsed Lasers," *Applied Optics*, Vol. 35, No. 6, 1996, pp. 948–964.

[14]McKenzie, R. L., "Planar Doppler Velocimetry Performance in Low-Speed Flows," AIAA Paper 97-0948, 1997.

[15]Smith, M. W., Northam, G. B., and Drummond, J. P., "Application of Absorption Filter Planar Doppler Velocimetry to Sonic and Supersonic Jets," *AIAA Journal*, Vol. 34, No. 3, 1996, pp. 434–441.

[16]Smith, M. W., "Application of a Planar Doppler Velocimetry System to a High Reynolds Number Compressible Jet," AIAA Paper 98-0428, 1998.

[17]Clancy, P. S., and Samimy, M., "Two-Component Planar Doppler Velocimetry in High-Speed Flows," *AIAA Journal*, Vol. 35, No. 11, 1997, pp. 1729–1738.

[18]Clancy, P. S., Samimy, M., and Erskine W. R., "Planar Doppler Velocimetry: Three-Component Velocimetry in Supersonic Jets," AIAA Paper 98-0506, 1998.

[19]Clancy, P., Samimy, M., and Erskine, W. R., "Planar Doppler Velocimetry: Three-Component Velocimetry in Supersonic Jets," *AIAA Journal*, Vol. 37, No. 6, 1999, pp. 700–707.

[20]Elliott, G. S., Mosedale, A., Gruber, M. R., Nejad, A. S., and Carter, C. D., "The Study of a Transverse Jet in a Supersonic Crossflow Using Molecular Filtered Based Diagnostics," AIAA Paper 97-2999, 1997.

[21]Mosedale, A. D., Elliott, G. S., Carter, C. D., and Beutner, T. J., "Planar Doppler Velocimetry: Toward Turbulence Measurements," *Proceedings of 1998 American Society of Mechanical Engineers Fluids Engineering Summer Meeting*, 1998.

[22]Mosedale, A., Elliott, G. S., Carter, C. D., and Beutner, T. J., "On the Use of Planar Doppler Velocimetry," AIAA Paper 98-2809, June 1998.

[23]Arnette, S. A., Elliott, G. S., Mosedale, A. D., and Carter, C. D., "A Two-Color Approach to Planar Doppler Velocimetry," AIAA Paper 98-0507, 1998.

[24]Meyers, J. F., "Doppler Global Velocimetry: The Next Generation?," AIAA Paper 92-3897, 1992.

[25]Meyers, J. F., "Development of Doppler Global Velocimetry for Wind Tunnel Testing," AIAA Paper 94-2582, 1994.

[26]Meyers, J. F., "Application of Doppler Global Velocimetry to Supersonic Flows," AIAA Paper 96-2188, 1996.

[27]Meyers, J. F., Lee, J. W., Fletcher, M. T., and South, B. W., "Hardening Doppler Global Velocimetry Systems for Large Wind Tunnel Applications," AIAA Paper 98-2606, June 1998.

[28]Beutner, T. J., Baust, H. D., and Meyers, J. F., "Doppler Global Velocimetry Measurements of a Vortex-Tail Interaction," *Flow Visualization*, edited by J. P. Crowder, Vol. 7, Bagell House, Seattle, WA, 1995.

[29]Beutner, T. J., and Baust, H. D., "Recent Developments in Doppler Global Velocimetry," CP-601, AGARD, Sept. 1997.

[30]Beutner, T. J., Elliott, G., Mosedale, A., and Carter, C., "Doppler Global Velocimetry Applications in Large Scale Facilities," AIAA Paper 98-2608, June 1998.

[31]Beutner, T. J., Williams, G. W., Baust, H. D., Elliott, G. S., Crafton, J., and Carter, C. D., "Characterization and Applications of Doppler Global Velocimetry," AIAA Paper 99-0266, Jan. 1999.

[32]Thorpe, S. J., Ainsworth, R. W., and Manners, R. J., "Time Averaged Free-Jet Measurements Using Doppler Global Velocimetry," *Proceedings of Fluid Engineering Division Summer Meeting*, FED Vol. 4, American Society of Mechanical Engineers, Fairfield, NJ, 1996, pp. 59–65.

[33]Roehle, I., Willert, C., and Schodl, R., "Application of Three-Dimensional Doppler Global Velocimetry in Turbo-Machinery," 8th International Symposium on Flow Visualizations, 1998.

[34]Stier, B., and Koochesfahani, M. M., "Molecular Tagging Velocimetry Developments in Gas Phase Flows," *Experiments in Fluids*, Vol. 23, Aug. 1997, pp. 361–372.

[35]Miles, R. B., and Lempert, W. R., "Quantitative Flow Visualization in Unseeded Flows," *Annual Review of Fluid Mechanics*, Vol. 29, 1997, pp. 285–326.

[36]Ribarov, L. A., Wehrmeyer, J. A., Batiwala, F., Pitz, R. W., and DeBarber, P. A., "Ozone Tagging Velocimetry Measurements Using Narrowband Excimer Lasers," AIAA Paper 98-0513, 1998.

[37]Adrian, R. J., "Particle-Imaging Techniques for Experimental Fluid Mechanics," *Annual Review of Fluid Mechanics*, Vol. 23, 1991, pp. 261–304.

[38]Grant, I., "Particle Imaging Velocimetry: a Review," *Proceedings of the Institute of Mechanical Engineers*, Vol. 211, Pt. C, 1997, pp. 55–76.

[39]Dahm, W. J. A., Su, L., and Southerland, K. B., "A Scalar Imaging Velocimetry Technique for Fully Resolved Four-Dimensional Vector Velocity Field Measurements in Turbulent Flows," *Physics of Fluids A*, Vol. 4, Oct. 1992, pp. 2191–2206.

[40]Su, L. K., and Dahm, W. J. A., "Scalar Imaging Velocimetry Measurements of the Velocity Gradient Tensor Field in Turbulent Flows. II. Experimental Results," *Physics of Fluids*, Vol. 8, July 1996, pp. 1883–1906.

[41]Elena, M., Lacharme, J. P., and Gaviglio, J., "Comparison of Hot-Wire and Laser Doppler Anemometry Methods in Supersonic Tabule Boundary Layers," *International Symposium on Laser Anemometry*, FED Vol. 33, American Society of Mechanical Engineers, New York, 1985, pp. 159–166.

[42]Samimy, M., Petrie, H. L., and Addy, A. L., "A Study of Compressible, Turbulent, Reattaching Free Shear Layers," *AIAA Journal*, Vol. 24, No. 2, 1986, pp. 261–267.

[43]Petrie, H. L., Samimy, M., and Addy, A. L., "Laser Doppler Velocimetry Bias in Separated Turbulent Flows," *Journal of Experiments in Fluids*, Vol. 6, No. 2, 1988, pp. 80–88.

[44]Samimy, M., and Elliot, G. S., "Effects of Compressibility on the Characteristics of Free Shear Layers," *AIAA Journal*, Vol. 28, No. 3, 1990, pp. 439–445.

[45]Goebel, S. G., and Dutton, C. J., "Experimental Study of Compressible Turbulent Mixing Layers," *AIAA Journal*, Vol. 29, No. 4, 1991, pp. 538–546.

[46]Bur, R., Corbel, B., and Delery, J., "Study of Passive Control in a Transonic Shock Wave/Boundary-Layer Interaction," *AIAA Journal*, Vol. 36, No. 3, 1998, pp. 394–400.

[47]Ross, C. B., Lourenco, L. M., and Krothapalli, A., "Particle Image Velocimetry Measurements in a Shock-Containing Supersonic Flow," AIAA Paper 94-0047, 1994.

[48]Urban, W. D., and Mungal, M. G., "Planar Velocimetry Measurements in Compressible Mixing Layers," AIAA Paper 97-0757, Jan. 1997.

[49]Urban, W. D., Watanabe, S., and Mungal, M. G., "Velocity Field of the Planar Shear Layer: Compressibility Effects," AIAA Paper 98-0697, Jan. 1998.

[50]Beresh, S. J., Comninos, M., Clemens, N. T., and Dolling, D. S., "The Effects of the Incoming Turbulent Boundary-Layer Structure on a Shock-Induced Separated Flow," AIAA Paper 98-0620, 1998.

[51]Wernet, M. P., "Stereo Viewing Three-Component, Planar PIV Utilizing Fuzzy Inference," *Proceedings of the 19th AIAA Conference on Advanced Measurement and Ground Testing Technology*, AIAA, Reston, VA, 1996.

[52]Shimizu, H., Lee, S., and She, C., "High Spectral Resolution LIDAR System with Atomic Blocking Filters for Measuring Atmospheric Parameters," *Applied Optics*, Vol. 22, May 1983, pp. 1373–1381.

[53]Shimizu, H., Noguchi, K., and She, C., "Atmospheric Temperature Measurement by a High Spectra Resolution LIDAR," *Applied Optics*, Vol. 25, No. 9, 1986, pp. 1460–1466.

[54]Miles, R. B., and Lempert, W. R., "Flow Diagnostics in Unseeded Air," AIAA Paper 90-0624, 1990.

[55]Miles, R. B., Lempert, W. R., and Forkey, J. N., "Instantaneous Velocity Fields and Background Suppression by Filtered Rayleigh Scattering," AIAA Paper 91-0357, 1991.

[56]Miles, R. B., Forkey, J. N., and Lempert, W. R., "Filtered Rayleigh Scattering Measurements in Supersonic/Hypersonic Facilities," AIAA Paper 92-3894, 1992.

[57]Forkey, J., Finkelstein, N. D., Lempert, W. R., and Miles, R. B., "Control of Experimental Uncertainties in Filtered Rayleigh Scattering Measurements," AIAA Paper 95-0298, 1995.

[58]Seasholtz, R. G., and Buggele, A. E., "Improvement in Suppression of Pulsed ND:YAG Laser Light with Iodine Absorption Cells for Filtered Rayleigh Scattering Measurements," NASA TM 113177, Nov. 1997.

[59]Finkelstein, N. D., Lempert, W. R., and Miles, R. B., "A Narrow Passband, Imaging, Refluorescence Filter for Nonintrusive Flow Diagnosics," AIAA Paper 96-2269, 1996.

[60]Finkelstein, N. D., Lempert, W. R., and Miles, R. B., "Mercury Vapor Filter Technology and Ultraviolet Laser Source for Flowfield Imaging," AIAA Paper 97-0157, 1997.

[61]Sabbaghzadeh, J., Buell, W., Holder, J., and Fink, M., "A Very Narrow, High Throughput Rayleigh Filter for Raman Spectroscopy," *Applied Physics B*, Vol. 60, 1995, pp. 261–265.

[62]Varghese, P., Phadke, C., and Fink, M., "A Novel Raman Technique for Flow Diagnostics," AIAA Paper 96-0302, 1996.

[63]Forkey, J., Cogne, A., Smits, Bogdonoff, S., Lempert, W. R., and Miles, R. B., "Time-Sequenced and Spectrally Filtered Rayleigh Imaging of Shock Wave and Boundary Layer Structure for Inlet Characterization," AIAA Paper 93-2300, 1993.

[64]Elliott, G. S., Samimy, M., and Arnette, S. A., "The Characteristics and Evolution of Large Scale Structures in Compressible Mixing Layers," *Physics of Fluids*, Vol. 7, April 1995, pp. 864–876.

[65]Arnette, S. A., Samimy, M., and Elliott, G. S., "Structure of Supersonic Turbulent Boundary Layer After Expansion Regions," *AIAA Journal*, Vol. 33, No. 3, 1995, pp. 430–438.

[66]Shirley, J. A., and Winter, M., "Air-Mass Flux Measurement System Using Doppler-Shifted Filtered Rayleigh Scattering," AIAA Paper 93-0513, 1993.

[67]Elliott, G. S., and Samimy, M., "Rayleigh Scattering Technique for Simultaneous Measurements of Velocity and Thermodynamic Properties," *AIAA Journal*, Vol. 34, No. 11, 1996, pp. 2346–2352.

[68]Forkey, J. N., "Development and Demonstration of Filtered Rayleigh Scattering—a Laser Based Flow Diagnostic for Planar Measurements of Velocity, Temperature, and Pressure," Final TR for NASA Graduate Student Researcher Fellowship Grant NGT-50826, Princeton Univ., Princeton, NJ, 1996.

[69]Clancy, P. S., "Development and Application of Three-Component Planar Doppler Velocimetry for High Speed Flows," Ph.D. Dissertation, Dept. of Mechanical Engineering, Ohio State Univ., Columbus, OH, 1997.

[70]Thermodynamics Research Center, "Thermodynamics Tables—Non-Hydrocarbons," TR, Texas A&M Univ., College Station, TX, 1975.

[71]Kuhlman, J., Naylor, S., James, K., and Ramanath, S., "Accuracy Study of a Two-Component Point Doppler Velocimeter," AIAA Paper 97-1916, 1997.

[72]Samimy, M., Kim, J.-H., Clancy, P., and Martens, S., "Passive Control of Supersonic Rectangular Jets via Trailing Edge Modifications," *AIAA Journal*, Vol. 36, No. 7, 1998, pp. 1230–1239.

[73]Adrian, R. J., and Yao, C. S., "Pulsed Laser Technique Application to Liquid and Gaseous Flows and the Scattering Power of Seed Materials," *Applied Optics*, Vol. 24, Jan. 1985, pp. 44–52.

[74]Melling, A., "Seeding Gas Flows for Laser Anemometry," *Propulsion and Energetics Panel 67th Symposium*, CP-399, AGARD, 1986.

[75]Meyers, J. F., "Generation of Particles and Seeding," Lecture Series 1991-08, von Kármán Inst., 1991.

[76]Samimy, M., and Abu-Hijleh, B. A. K., "Performance of LDV with Polydisperse Seed Particles in High Speed Flows," *Journal of Propulsion and Power*, Vol. 5, No. 1, 1989, pp. 21–25.

[77]Samimy, M., and Langenfeld, C. A., "Experimental Study of Isothermal Swirling Flows in a Dump Combustor," *AIAA Journal*, Vol. 26, No. 12, 1988, pp. 1442–1449.

[78]Gouldin, F. C., Depsky, J. S., and Lee, S.-L., "Velocity Field Characteristics of a Swirling Flow Combustor," *AIAA Journal*, Vol. 23, No. 1, 1985, pp. 95–102.

[79]Wernet, J. H., and Wernet, M. P., "Stabilized Alumina/Ethanol Colloidal Dispersion Technique for Seeding High Temperature Flows," NASA TM 106591, 1994.

[80]Wernet, M. P., Skoch, G. J., and Wernet, J. H., "Demonstration of a Stabilized Alumina/Ethanol Colloidal Dispersion Technique for Seeding High Temperature Flows," NASA TM 106945, 1995.

[81]Maxwell, B. R., and Seasholtz, R. G., "Velocity Lag of Solid Particles in Oscillating Gases and in Gases Passing Through Normal Shock Waves," NASA TN D-7490, March 1974.

[82]Melling, A., "Tracer Particles and Seeding for Particle Image Velocimetry," *Measurement Science and Technology*, Vol. 8, Dec. 1997, pp. 1406–1416.

[83]Crowe, C. T., Gore, R. A., and Troutt, T. R., "Particle Dispersion by Coherent Structures in Free Shear Flows," *Particle Science and Technology*, Vol. 3, 1985, pp. 149–158.

[84]Samimy, M., and Lele, S. K., "Motion of Particles with Inertia in a Compressible Shear Layer," *Physics of Fluids A*, Vol. 3, Aug. 1991, pp. 1915–1923.

[85]Fowles, G. R., *Introduction to Modern Optics*, 2nd ed., Dover, New York, 1989.

[86]Eckbreth, A., *Laser Diagnostics for Combustion Temperature and Species*, 2nd ed., Gordon and Breach, Amsterdam, 1996.

[87]Smith, M. W., "The Reduction of Laser Speckle Noise in Planar Doppler Velocimetry Systems," AIAA Paper 98-2607, June 1998.

[88]Clancy, P. S., and Samimy, M., "Velocity and Vorticity Measurements in Supersonic Jets Modified with a Vortex Generating Tab," *Proceedings of 1998 ASME Fluids Engineering Summer Meeting*, American Society of Mechanical Engineers, Fairfield, NJ, 1998.

[89]Samimy, M., Zaman, K. B. M. Q., and Reeder, M. F., "Effect of Tabs on the Flow and Noise Field of an Axisymmetric Jet," *AIAA Journal*, Vol. 6, No. 4, 1993, pp. 778–793.

[90]Zaman, K. M. B. Q., Reeder, M. F., and Samimy, M., "Control of an Axisymmetric Jet Using Vortex, 1985 Generators," *Physics of Fluids*, Vol. 6, Feb. 1994, pp. 778–793.

[91]Reeder, M. F., and Samimy, M., "The Evolution of a Jet with Vortex-Generating Tabs: Visualization and Analysis of Mean and Instantaneous Properties," *Journal of Fluid Mechanics*, Vol. 311, 1996, pp. 73–118.

[92]Arroyo, M. P., and Greated, C. A., "Stereoscopic Particle Image Velocimetry," *Measurement Science and Technology*, Vol. 2, Dec. 1991, pp. 1181–1186.

[93]Westerweel, J., and Nieuwstadt, F. T. M., "Performance Tests on 3-Dimensional Velocity Measurements with A Two-Camera Digital Particle-Image Velocimeter," *ASME Fourth International Conference on Laser Anemometry*, Cleveland, OH, 1991.

[94]Grant, I., Fu, S., Pan, X., and Wang, X., "The Application of an In-Line, Stereoscopic, PIV System to 3-Component Velocity Measurements," *Experiments in Fluids*, Vol. 19, 1995, pp. 214–221.

[95]Laufer, G., *Optics and Lasers in Engineering*, Cambridge Univ. Press, New York, 1996.

[96]Fujii, H., and Asakura, T., "Effect of Surface Roughness on the Statistical Distribution of Image Speckle Intensity," *Optics Communications*, Vol. 11, No. 1, 1974, pp. 35–38.

[97]Fujii, H., and Asakura, T., "A Contrast Variation of Image Speckle Intensity Under Illumination of Partially Coherent Light," *Optics Communications*, Vol. 12, No. 1, 1974, pp. 33–38.

[98]Ohtsubo, J., and Asakura, T., "Measurements of Surface Roughness Properties Using Speckle Patterns with Non-Gaussian Statistics," *Optics Communications*, Vol. 25, No. 3, 1978, pp. 315–319.

[99]Dainty, J. C., "Introduction," *Laser Speckle and Related Phenomena*, edited by J. C. Dainty, Vol. 9, Topics in Applied Physics, Springer–Verlag, Berlin, 1984, pp. 1–7.

[100]Goodman, J. W., "Statistical Properties of Laser Speckle Patterns," *Laser Speckle and Related Phenomena*, edited by J. C. Dainty, Vol. 9, Topics in Applied Physics, Springer–Verlag, Berlin, 1984, pp. 9–75.

[101]Arsenault, H. H., and April, G., "Properties of Speckle Integrated with a Finite Aperture and Logarithmically Transformed," *Journal of the Optical Society of America*, Vol. 66, No. 11, 1976, pp. 1160–1163.

[102]Ennos, A. E., "Speckle Interferometry," *Laser Speckle and Related Phenomena*, 2nd ed., edited by J. C. Dainty, Vol. 9, Topics in Applied Physics, Springer–Verlag, Berlin, 1984, pp. 207–209.

[103]Wernet, M. P., "Fuzzy Inference Enhanced Information Recovery from Digital PIV Using Cross-Correlation Combined with Particle Tracking," *SPIE Conference on Optical Diagnostics in Fluid and Thermal Flow*, Vol. 2546, 1995, pp. 54–64.

[104]Raffel, M., Willert, C., and Kompenhans, J., *Particle Image Velocimetry, A Practical Guide*, Springer, New York, 1998, p. 204.

[105]Wernet, M. P., "PIV for Turbomachinery Applications," NASA TM 107525, 1997.

[106]Adrian, R. J., "Multi-Point Optical Measurements of Simultaneous Vectors in Unsteady Flow-A Review," *International Journal of Heat and Fluid Flow*, Vol. 7, 1986, pp. 127–145.

[107]Landreth, C. C., Adrian, R. J., and Yao, C. S., "Double Pulsed Particle Image Velocimeter with Directional Resolution for Complex Flows," *Experiments in Fluids*, Vol. 6, No. 2, 1988, pp. 119–128.

[108]Kompenhans, J., and Raffel, M., "The Importance of Image Shifting to the Applicability of the PIV Technique for Aerodynamic Investigations," *Seventh International Symposium on Applications of Laser Techniques to Fluid Mechanics*, 1994, pp. 35.6.1–35.6.6.

[109]Raffel, M., and Kost, F., "Investigation of Aerodynamic Effects of Coolant Ejection at the Trailing Edge of a Turbine Blade Model by PIV and Pressure Measurements," *Experiments in Fluids*, Vol. 24, No. 5/6, 1998, pp. 447–461.

[110]Krothapalli, A., Wishart, D. P., and Lourenco, L. M., "Near Field Structure of a Supersonic Jet: 'On-Line' PIV Study," *Seventh International Symposium on Applications of Laser Techniques to Fluid Mechanics*, 1994, pp. 26.5.1–26.5.6.

[111]Wernet, M. P., "Digital PIV Measurements in the Diffuser of a High Speed Centrifugal Compressor," AIAA Paper 98-2777, June 1998.

[112]Wernet, M. P., "Particle Displacement Tracking Applied to Air Flows," *ASME Fourth International Conference on Laser Anemometry*, 1991, pp. 327–335.

[113]Bryanston-Cross, P. J., Towers, C. E., Judge, T. R., Towers, D. P., Harasgama, S. P., and Hopwood, S. T., "The Application of Particle Image Velocimetry (PIV) in a Short-Duration Transonic Annular Turbine Cascade," *Transactions of the American Society of Mechanical Engineers*, Vol. 114, July 1992, pp. 504–509.

[114]Chana, K. S., Healy, N., and Bryanston-Cross, P. J., "Particle Image Velocimetry Measurements from the Stator–Rotor Interaction Region of a High Pressure Transonic Turbine Stage at the DERA Isentropic Light Piston Facility," CP-598, AGARD, AGARD/PEP 90th Symposium on Advanced Non-Intrusive Instrumentation for Propulsion Engines, 1997, pp. 46.1–46.8.

[115]Wernet, M. P., "Fuzzy Logic Particle-Tracking Velocimetry," *SPIE Conference on Optical Diagnostics in Fluid and Thermal Flow*, Vol. 2005, 1993, pp. 701–708.

[116]Cenedese, A., Paglialunga, A., Romano, G. P., and Terlizzi, M., "Neural Net for Trajectories Recognition in a Flow," *Sixth International Symposium on Applications of Laser Techniques to Fluid Mechanics*, 1992, pp. 27.1.1–27.1.5.

[117]Keane, R. D., Adrian, R. J., and Zhang, Y., "Super-Resolution Particle Imaging Velocimetry," *Measurement Science and Technology*, Vol. 6, No. 6, 1995, pp. 754–768.

[118]Post, M. E., Goss, L. P., and Brainard, L. F., "Two-Color Particle Imaging Velocimetry in a Turbine Cascade," AIAA Paper 91-0274, Jan. 1991.

[119]Estevadeoral, J., Gogineni, S., Copenhaver, W., Bloch, G., and Brendel, M., "Flow Structure in a Low-Speed Axial Fan: a DPIV Investigation," AIAA Paper 98-2905, June 1998.

[120]Wernet, M. P., "Demonstration of PIV in a Transonic Compressor," CP-598, AGARD, 1997, pp. 51.1–51.13.

[121]Kooi, J. W., Pengel, K., Raffel, M., Willert, C., and Kompenhans, J., "Application of PIV in the Large Low Speed Facility of DNW," CP-601, AGARD, 1997, pp. 5.1–5.12.

[122]Westerweel, J., "Fundamentals of Digital Particle Image Velocimetry," *Measurement Science and Technology*, Vol. 8, No. 12, 1997, pp. 1379–1392.

[123]Wernet, M. P., and Pline, A., "Particle Displacement Tracking Technique and Cramer–Rao Lower Bound Error in Centroid Estimates from CCD Imagery," *Experiments in Fluids*, Vol. 15, No. 4/5, 1993, pp. 295–307.

[124] Okamoto, K., Hassan, Y. A., and Schmidl, W. D., "Simple Calibration Technique Using Image Cross-Correlation for Three Dimensional PIV," *Flow Visualization and Image Processing of Multiphase Systems*, FED Vol. 209, American Society of Mechanical Engineers, Fairfield, NJ, 1995, pp. 99–106.

[125] Hinsch, K. D., "Three-Dimensional Particle Velocimetry," *Measurement Science and Technology*, Vol. 6, No. 6, 1995, pp. 742–753.

[126] Brucker, C., "3-D Scanning Particle Image Velocimetry: Technique and Application of Dual Color-Light-Sheet Scanning," *Proceedings of the 8th International Symposium on Laser Anemometry*, 1995, pp. 4.2.1–4.2.7.

[127] Brucker, C., "3-D Scanning PIV Applied to an Air Flow in a Motored Engine Using Digital High Speed Video," *Measurement Science and Technology*, Vol. 8, No. 12, 1997, pp. 1480–1492.

[128] Gauthier, V., and Riethmuller, M. L., "Particle Image Velocimetry," Lecture Series 1988-06, N89-17179, von Kármán Inst. for Fluid Dynamics, 1988.

[129] Prasad, A. K., and Adrian, R. J., "Stereoscopic Particle Image Velocimetry Applied to Liquid Flows," *Sixth International Symposium on Applications of Laser Techniques to Fluid Mechanics*, 1992, pp. 6.1.1–6.1.8.

[130] Kingslake, R., *Optics in Photography*, Society of Photo-Optical Instrumentation Engineers Optical Engineering Press, Bellingham, WA, 1992.

[131] Funes-Gallanzi, M., and Bryanston-Cross, P. J., "Solid State Visualization of a Highly Three Dimensional Flow Using Stereoscopic Particle Image Velocimetry (3DPIV)," *SPIE Conference on Optical Diagnostics in Fluid and Thermal Flow*, Vol. 2005, 1993, pp. 360–369.

[132] Wernet, M. P., and Pline, A., "Particle Image Velocimetry for the Surface Tension Driven Convection Experiment Using a Particle Displacement Tracking Technique," *ASME Fourth International Conference on Laser Anemometry*, 1991, pp. 315–325.

R. P. Lucht
Associate Editor